https://doi.org/10.5194/egusphere-2025-2408
Preprint. Discussion started: 17 July 2025


# Climate-related signals in the GV7-C ice core from East Antarctica for 1782–2013 CE: Potential relevance to climate and teleconnections between tropics and Antarctica

Yalalt Nyamgerel[1], Yeongcheol Han[2], Soon Do Hur[2], Hyemi Kim[1], Songyi Kim[1,2], Jangil Moon[2], Barbara Stenni[3], Jeonghoon Lee[1]*

[1]Department of Science Education, Ewha Womans University, Seoul 120-750, Republic of Korea
[2]Division of Glacier and Earth Sciences, Korea Polar Research Institute, Incheon 21990, Republic of Korea
[3]Department of Environmental Sciences, Informatics and Statistics, Ca' Foscari University, Venice 30123, Italy

*Correspondence to*: Jeonghoon Lee (jeonghoon.d.lee@gmail.com)

**Abstract.** This study investigates climate-related signals preserved in the GV7-C ice core from East Antarctica (1782–2013 CE), analyzing stable water isotopes ($\delta^{18}O$ and d-excess) and snow accumulation (SA). Annual data were compared with climate indices representing the El Niño–Southern Oscillation (Niño3.4, SOI), Southern Annular Mode (SAM), Indian Ocean Dipole (IOD), and sea surface temperature (SST) anomalies in the southeastern Indian Ocean (SST-SEIO). During 1957–2013 CE, $\delta^{18}O$ correlated intermittently with Pacific Ocean sector indices, while d-excess consistently correlated with SAM, IOD, and SST-SEIO, indicating stable moisture sources from the Indian Ocean. Over the longer period (1872–2013 CE), $\delta^{18}O$ correlations weakened, suggesting shifting climatic influences, whereas d-excess retained correlations, emphasizing its reliability for tracking moisture-source variability. Snow accumulation showed weak and inconsistent correlations with climatic variables, suggesting multiple influencing factors. Spatial correlation analyses revealed that $\delta^{18}O$ and d-excess signals primarily reflect conditions in the Pacific and Indian Ocean sectors, respectively. These findings highlight dynamic teleconnections between Antarctic climate and tropical ocean conditions, underscoring the complexity of interpreting Antarctic ice core records in climate variability studies and emphasizing the importance of considering varying temporal resolutions and climatic contexts.

## 1 Introduction

Understanding climate variabilities over the Antarctic continent and the surrounding Southern Ocean is crucial for the global climate system (Mayewski et al., 2009; Fretwell et al., 2013; Rintoul et al., 2018). Large variations in the air temperature (Nicolas and Bromwich, 2014; Constable et al., 2022) and surface mass balance have been reported (Dalaiden et al., 2020a), reflecting the complex nature of the Antarctic climate (Masson-Delmotte et al., 2008). Sparse observational data and its high variability further contribute to these large variations (Kim et al., 2020; Klein et al., 2019). Particularly, climate conditions in coastal regions of Antarctica show notable variations (Tuohy et al., 2015; Stenni et al., 2017; Goursaud et al., 2019).

https://doi.org/10.5194/egusphere-2025-2408
Preprint. Discussion started: 17 July 2025


Antarctic ice core records reflect the past climatic and environmental conditions. The variations in the stable water isotopic compositions ($\delta^{18}O$ and $\delta D$) in ice cores are indicative of relative changes in the atmospheric temperature (Jouzel et al., 1997; Markle and Steig, 2022), sea ice extent (SIE), and atmospheric circulation (Thomas and Abram, 2016). In addition, the second-order parameter *d*-excess (*d*-excess = $\delta D - 8 \times \delta^{18}O$), which is sensitive to changes in the relative humidity and sea surface temperatures (SSTs) in the source region (Jouzel et al., 1982; Delmotte et al., 2000; Uemura et al., 2008), thus has been used to identify source regions (Stenni et al., 2001; Sodemann and Stohl., 2009). Furthermore, snow accumulation (SA) rates estimated from ice cores show a tendency to increase in warmer climates (Frieler et al., 2015; Palerme et al., 2017) and under low-sea ice conditions in coastal regions (Nyamgerel et al., 2020), being potential to reflect the surface air temperatures (Dalaiden et al., 2020a).

Changes in the atmospheric circulation pattern are influential on the stable water isotopic signals from ice cores (Bertler et al., 2004; Kino et al., 2021; Leroy-Dos Santos et al., 2023). Slowly varying large-scale atmospheric circulation and short-lived synoptic-scale events are known to be driving factors for the atmospheric moisture budget over Antarctica (Dalaiden et al., 2020b). The isotopic relationships to the surface air temperature and surface mass balance vary, depending on the relative contribution of large-scale atmospheric dynamical process and thermodynamic processes (Oerter et al., 2000; Medley et al., 2018, Goursaud et al., 2019; Dalaiden et al., 2020b). In recent decades, the Southern Annular Mode (SAM), which indicates the modulation of westerly winds towards the Southern Hemisphere (Hall and Visbeck, 2002; Fogt et al., 2012), has become increasingly important for the Southern Hemisphere climate (Russell and McGregor, 2010). The SAM affects the spatial patterns of variability in temperature, precipitation, and sea ice cover across Antarctica (Nicolas and Bromwich, 2014; Purich et al., 2016; Kim et al., 2020). In addition, evidence of SAM-related changes affecting $\delta^{18}O$ preserved in ice cores and the surface mass balance has been observed at the coastal East Antarctic sites (Schlosser et al., 2014; Servettaz et al., 2020). Teleconnections between the Antarctic ice core records and tropical climate variabilities have previously been reported (Yuan, 2004; Schneider and Steig, 2008). The Antarctic surface mass balance is also linked with El Niño-Southern Oscillation (ENSO) (Kim et al., 2020). However, the atmospheric and oceanic teleconnections between tropical and Antarctic regions are complex, limiting their detectability in ice cores (Divine et al., 2009; Turner et al., 2009). Moreover, the response of ENSO variability is unstable over time and depends on the time scales under consideration and the concurrent state of the ENSO and SAM (Divine et al., 2009). There remains considerable ambiguity regarding the geographical extent of climate signals derived from ice cores (Stenni et al., 2017). Indeed, considerable differences in both spatial and temporal variabilities indicate the need for regionally or locally focused studies and additional ice core records, particularly in the coastal East Antarctica (Vance et al., 2016; Goursaud et al., 2017). The GV7-C ice core site, known for its high SA, offers well-dated, and high-resolution data (Caiazzo et al., 2017; Nardin et al., 2021).

This study, thus, aimed to explore the climate-related signals in the GV7-C ice core record ($\delta^{18}O$, $\delta D$, *d*-excess, and SA rate) on an annual scale for the 1782–2013 CE period. The GV7-C ice core record was systematically compared with various climate variables at different time scales (annual and seasonal) because the isotopic signals recorded in an ice core reflect a broad range of parameters, including source conditions, transportation pathways, and rainout (Jackson et al., 2023). Particular

https://doi.org/10.5194/egusphere-2025-2408
Preprint. Discussion started: 17 July 2025


attention was given to potential remote influences from the ENSO and SAM, as suggested by a previous study covering the period from 1979 to 2012 CE (Khan, 2019). This study offers potential insights from the GV7-C ice core into the teleconnections between the tropics and high latitudes in the Southern Hemisphere.

## 2 Materials and methods

### 2.1 Study area

During the 2013/14 Antarctic summer season, a collaborative Italian/Korean expedition drilled several firn-ice cores at the GV7 drilling site (70°41′ S, 158°52′ E; 1950 m a.s.l.), located on the Oates Coast of East Antarctic (Fig. 1). Six shallow firn cores (ranging from 5 and 50 m in length) and intermediate firn-ice cores (ranging from 78 and 250 m in length) were drilled. The 78m deep core, named GV7-C, is used and presented in this study. The site is approximately 95 km away from the nearest coastline, and the ice velocity at this location is very low (< 0.3 m yr–1) (Frezzotti et al., 2007), and the 10-m firn temperature was measured to be –31.8 °C (Frezzotti et al., 2007). Notably, the SA rate in this area is relatively high, while the post-depositional effect is low due to the low intensity of katabatic winds along the ice divide (Becagli et al., 2004; Frezzotti et al., 2007; Magand et al., 2004). During the autumn–winter period, the air mass primarily originates from the western Pacific Ocean (PO) sector, while the spring period is characterized by dominant input from the Ross Sea sector, with prevailing winds from the south (Caiazzo et al., 2017). Back trajectory estimations conducted from 2007 to 2012 revealed that the dominant air mass pathways are from the Indian Ocean (IO) (32%) and the Antarctic Plateau (29%) (Caiazzo et al., 2017), while the Ross Sea and western PO sectors account for 21% and 19%, respectively. Furthermore, the western PO and IO sectors accounted for 59% (147 mm) and 28% (69 mm) of the total precipitation (250 mm), respectively (Caiazzo et al., 2017). The SA at this site was estimated to be higher in austral summer and autumn (Caiazzo et al., 2017). Notably, the western PO sector also exhibits a second maximum in winter, with the trajectory pathway indicating dominance from the Antarctica Plateau and the IO sector.

https://doi.org/10.5194/egusphere-2025-2408
Preprint. Discussion started: 17 July 2025


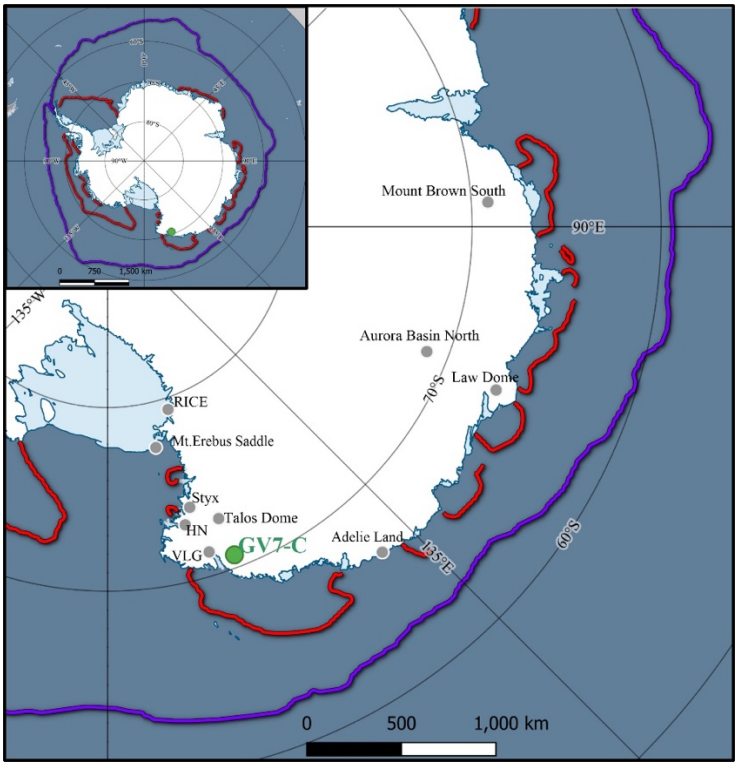


**Figure 1.** Location of the GV7-C ice core and other ice core sites in East Antarctica. The red lines indicate the median sea ice concentration in February and the purple line represents the same for September based on data from 1981–2010 CE (Fetterer et al., 2016). The map was generated using QGIS software with Quantarctica3 project data (Matsuoka et al., 2021).

### 2.2 Ice core data

The 78 m long GV7-C ice core was collected over a total of 107 runs, and the average diameter of the ice core was measured to be an average diameter of 0.08 m. Density was estimated by measuring the mass and dimensions of the ice core subsections. The ice core sections were kept frozen and transported to Korea. Inside the cold room at the Korea Polar Research Institute (KOPRI), the ice core sections were cut to an average length of 0.04 m for stable water isotopic analysis ($\delta^{18}O$ and $\delta D$). A total of 1880 samples were analyzed using cavity ring-down spectrometers (L2130-I and L2140-i, Picarro Inc., USA) at KOPRI. Annual layers were determined based on the seasonal summer maximum $\delta^{18}O$ peaks in the GV7-C ice core and the age of each sample depth was determined by interpolation between two consecutive peaks. The GV7-C ice core covers the period from 1782 to 2014 CE. The seasonal $\delta^{18}O$ pattern has been reported in previous studies (Caiazzo et al., 2017; Nardin et al., 2021). The annual layer counting of the ice core was confirmed and further constrained using the electrical conductivity peaks of Pinatubo (1991 CE), Agung (1963 CE), Tarawera (1886 CE), Krakatau (1883 CE), and Tambora (1815 CE). The annual mean

https://doi.org/10.5194/egusphere-2025-2408
Preprint. Discussion started: 17 July 2025


SA rate was calculated by multiplying the depth corresponding to one full year by the density and was expressed in millimeters of water equivalent per year (mm w.e. yr–1). The *d*-excess (*d*-excess = $\delta D - 8 \times \delta^{18}O$) was also calculated.

### 2.3 Climate data and analysis

The annual means of $\delta^{18}O$, *d*-excess, and SA in the GV7-C ice core were used in the analysis for different time periods. Spatial correlation analysis was conducted using gridded climate data from the ERA5 reanalysis (air temperature, SST, sea ice concentration [SIC], 10-m wind speed, zonal [u] and meridional [v] wind components, geopotential height [GPH] changes, total precipitation, and total precipitable water) for the 1957–2013 CE period using Climate Reanalyzer developed by the University of Maine, USA (https://climatereanalyzer.org/). The correlation results were examined on both an annual and seasonal scale (DJF, MAM, JJA, and SON) at different pressure levels (surface, 850 hPa, 500 hPa, and 250 hPa), and significant correlations are selectively presented. Various climate indices were compared with the GV7-C ice core records; station-based SAM index for 1957–2013 CE (Marshall G and National Center for Atmospheric Research Staff, 2018), reconstructed SAM index for 1872–2013 CE (https://psl.noaa.gov/data/20thC_Rean/timeseries/monthly/SAM), the Southern Oscillation Index (SOI) (https://www.ncei.noaa.gov/access/monitoring/enso/soi), Niño 3.4 index (https://psl.noaa.gov/gcoswgsp/Timeseries/Nino34), the SST anomaly over the southeastern equatorial IO (SST-SEIO) (90°E–110°E and 10°S–0°N) and Indian Ocean Dipole (IOD) index for 1870–2013 CE, which represents the SST gradient between the western (50°E–70°E and 10°S–10°N) and the southeastern equatorial IO (https://psl.noaa.gov/gcos_wgsp/Timeseries/DMI), and the reconstructed SIE over the Ross-Amundsen Sea sector (162°E–250°E) and the East Antarctic sector (71°E–162°E) (Fogt et al., 2023). The reconstructed SST data for 1872–2013 CE (https://www.ncei.noaa.gov/access/monitoring/climate-at-a-glance/global/time-series) (Huang et al., 2017) was also compared with the ice core data. Linear correlations were determined using Pearson's correlation coefficient (r). Principal component analysis (PCA), a linear dimensionality reduction technique, was employed to investigate any similarities in the variation within the ice core and climate datasets.

## 3 Results

### 3.1 Characterization of the GV7-C ice core record

The descriptive statistics for the annual mean $\delta^{18}O$, $\delta D$, *d*-excess, and SA in the GV7-C ice core are presented in Table 1. The annual mean $\delta^{18}O$ in the GV7-C ice core (n = 233) fluctuated between –32.92‰ and –24.60‰ for the 1782–2013 CE period, while $\delta D$ ranged from –259.42‰ to –210.21‰. The long-term means of $\delta^{18}O$, *d*-excess, and SA did not exhibit any significant differences between the time periods, except for *d*-excess in 1982–2013 CE (Table 1).

The annual variation in $\delta^{18}O$, *d*-excess, and SA is presented in Figure 2, revealing large interannual and decadal-scale variations. Sequential years (at least five) with smaller (or colder) than average $\delta^{18}O$ (–29.64‰) were observed for six periods (1838–1842 CE, 1858–1862 CE, 1880–1885 CE, 1904–1908 CE, 1918–1922 CE, 1960–1965 CE, and 1995–2002 CE). Additionally,

https://doi.org/10.5194/egusphere-2025-2408
Preprint. Discussion started: 17 July 2025


the years between 1977 and 1991 were lower than average, except for 1979, 1982, 1985, and 1990. In addition, sequential years (at least six) higher than the average were observed for 1787–1801, 1807–1813, 1937–1942, and 1948–1958 (except 1953) (Fig. 2). The linear relationship between $\delta^{18}O$ and $\delta D$ ($\delta D = 8.46 \times \delta^{18}O + 17.97$, R2 = 0.99, n = 1880, $p < 0.001$) had a slope slightly larger than that for the precipitation isotopic composition both globally (8) (Craig, 1961) and on the Antarctic–wide scale (7.75) (Masson-Delmotte et al., 2008). The slopes derived for the different time scales ranged from 8.35 (for 1982–2013) to 8.67 (for 1882–1931) (Table 2).

The annual *d*-excess ranged between 1.70‰ and 7.61‰ (n = 233) (Table 1). Periods with values larger than the mean for at least five sequential years were observed for 1786–1790 CE, 1855–1861 CE, 1884–1888 CE, 1903–1911 CE, 1932–1940 CE, 1951–1956 CE, 1962–1966 CE, and 1974–1978 CE, while years with lower values than the mean for at least five sequential years occurred in 1798–1802 CE, 1840–1848 CE, 1922–1926 CE, 1985–1990 CE, and 2006–2011 CE (Fig. 2). A positive correlation was observed between $\delta^{18}O$ and *d*-excess (r = 0.45, $p < 0.001$, n = 1880) (Table 3), indicating their relevance to the climatic conditions in the moisture source region. The slopes for the relationship between *d*-excess and $\delta^{18}O$ varied slightly between different time periods, though positive correlations were consistently maintained over these periods (Table 3). This suggests a relatively consistent supply of the air mass source (i.e., oceanic) to the GV7-C site. Thus, it can be assumed that the variation in $\delta^{18}O$ and *d*-excess in the GV7-C ice core is indicative of the oceanic surface conditions (e.g., humidity, SST, and wind speed) (Uemura et al., 2008).

The annual mean SA ranged from 79 to 460 mm w.e. yr–1 in the GV7-C ice core, with a long-term mean of 223 ± 59 mm w.e. yr–1 (Table 1). Strong interannual variation was observed, with no long-term trend over the 1782–2013 CE period. Consecutive years (at least four) with a SA larger than the mean (223 mm w.e. yr–1) were observed in 1784–1787 CE, 1896–1899 CE, and 1999–2002 CE, while the 1878–1883 CE and 1945–1952 CE periods exhibited a lower SA rate than the mean (Fig. 2). The mean SA in the GV7-C ice core was comparable to previously reported records nearby and in other coastal regions across East Antarctica (Table 4).

https://doi.org/10.5194/egusphere-2025-2408
Preprint. Discussion started: 17 July 2025


**Table 1.** Descriptive statistics for the annual means of the GV7-C ice core data.

| Years (CE) | Long-term (1782–2013) | 1782–1831 | 1832–1881 | 1882–1931 | 1932–1981 | 1982–2013 |
|---|---|---|---|---|---|---|
| | | | $\delta^{18}O$ (‰) | | | |
| Mean | –29.64 | –29.24 | –29.78 | –29.88 | –29.49 | –29.90 |
| Standard Deviation | 1.26 | 1.02 | 1.41 | 1.09 | 1.28 | 1.45 |
| Minimum | –32.92 | –32.72 | –32.92 | –32.34 | –32.74 | –31.96 |
| Maximum | –24.60 | –26.86 | –24.60 | –27.39 | –27.14 | –24.84 |
| | | | δD (‰) | | | |
| Mean | –232.69 | –229.59 | –233.76 | –234.69 | –231.76 | –234.17 |
| Standard Deviation | 10.37 | 8.42 | 11.50 | 9.31 | 10.50 | 11.91 |
| Minimum | –259.42 | –259.42 | –258.36 | –255.61 | –258.98 | –250.66 |
| Maximum | –191.43 | –210.21 | –191.43 | –213.50 | –212.01 | –192.08 |
| | | | *d*-excess (‰) | | | |
| Mean | 4.43 | 4.33 | 4.44 | 4.36 | 4.20 | 5.02 |
| Standard Deviation | 1.07 | 0.88 | 1.08 | 1.25 | 1.03 | 0.97 |
| Minimum | 1.70 | 2.25 | 2.21 | 1.70 | 2.42 | 2.98 |
| Maximum | 7.61 | 6.34 | 6.99 | 7.61 | 7.07 | 6.64 |
| | | | Snow accumulation (mm w.e. $yr^{-1}$) | | | |
| Mean | 223.01 | 225.06 | 217.80 | 227.03 | 219.76 | 226.70 |
| Standard Deviation | 58.77 | 68.97 | 48.93 | 54.91 | 59.15 | 63.50 |
| Minimum | 79.02 | 101.79 | 143.06 | 81.37 | 107.58 | 79.02 |
| Maximum | 459.88 | 459.88 | 307.94 | 319.04 | 340.61 | 343.92 |

https://doi.org/10.5194/egusphere-2025-2408
Preprint. Discussion started: 17 July 2025


**Table 2.** Linear regression analysis for $\delta^{18}O$ and $\delta D$ from the GV7-C ice core.

| | Slope | Intercept | $R^2$ | *p*-value | n |
|---|---|---|---|---|---|
| All data | 8.46 | 17.97 | 0.99 | <0.0001 | 1880 |
| Annual mean | 8.17 | 9.64 | 0.99 | <0.0001 | 233 |
| Annual maximum | 8.27 | 13.57 | 0.98 | <0.0001 | 233 |
| Annual minimum | 8.19 | 9.07 | 0.99 | <0.0001 | 233 |
| 1782–1831 CE | 8.54 | 20.12 | 0.99 | <0.0001 | 344 |
| 1832–1881 CE | 8.44 | 17.60 | 0.99 | <0.0001 | 355 |
| 1882–1931 CE | 8.67 | 24.36 | 0.99 | <0.0001 | 399 |
| 1932–1981 CE | 8.51 | 19.41 | 0.99 | <0.0001 | 429 |
| 1982–2013 CE | 8.35 | 15.51 | 0.99 | <0.0001 | 353 |

https://doi.org/10.5194/egusphere-2025-2408
Preprint. Discussion started: 17 July 2025


**Table 3.** Linear regression analysis for $\delta^{18}O$ and d-excess from the GV7-C ice core.

| | Slope | Intercept | $R^2$ | *p*-value | n |
|---|---|---|---|---|---|
| All data | 0.46 | 18.07 | 0.21 | <0.0001 | 1880 |
| Annual mean | 0.18 | 9.68 | 0.04 | <0.0001 | 233 |
| Annual maximum | 0.28 | 14.45 | 0.10 | <0.0001 | 233 |
| Annual minimum | 0.26 | 10.68 | 0.09 | <0.0001 | 233 |
| 1782–1831 CE | 0.54 | 20.04 | 0.24 | <0.0001 | 344 |
| 1832–1881 CE | 0.45 | 17.83 | 0.18 | <0.0001 | 355 |
| 1882–1931 CE | 0.67 | 24.33 | 0.34 | <0.0001 | 399 |
| 1932–1981 CE | 0.52 | 19.45 | 0.24 | <0.0001 | 429 |
| 1982–2013 CE | 0.36 | 15.62 | 0.18 | <0.0001 | 353 |

https://doi.org/10.5194/egusphere-2025-2408
Preprint. Discussion started: 17 July 2025


**Table 4.** Comparison of the mean snow accumulation rate from the GV7-C ice core with previous ice core records in this location and other East Antarctic ice cores.

| Location | Approximate distance to GV7-C, km | Snow accumulation, mm w.e $yr^{-1}$ | Period (CE) | Reference |
|---|---|---|---|---|
| GV7-C | – | 223 ± 59 | 1782–2013 | This study |
| GV7 site | – | 252 ± 104 | 2001–2004 | Frezzotti et al., 2007 |
| GV7 site | – | 242 ± 71 | 2007–2013 | Caiazzo et al., 2017 |
| GV7 site | – | 250 ± 85 | 2008–2013 | Caiazzo et al., 2017 |
| GV7 site | – | 238.7 ± 13 | 1979–2012 | Khan, 2019 |
| GV7 site | – | 241 ± 13 | 1965–2001 | Magand et al., 2004 |
| GV7 site | – | 242 ± 57 | 1965–2000 | Nardin et al., 2021 |
| GV7 site | – | 233 ± 64 | 1854–2004 | Nardin et al., 2021 |
| GV7 site | – | 205 ± 63 | 1179–2009 | Nardin et al., 2021 |
| RICE | 972 | 210 | 1965–2017 | Winstrup et al., 2017 |
| Mt. Erebus Saddle | 811 | 230 | 1950–2006 | Rhodes et al., 2012 |
| Styx-B | 394 | 146 ± 60 | 1990–2014 | Nyamgerel et al., 2020 |
| Hercules Névé | 348 | 119 | 1770–1992 | Stenni et al., 1999 |
| VLG (Victoria Lower Glacier) | 155 | 30 | 1808–2000 | Bertler et al., 2011 |
| Talos Dome | 239 | 80 | 1232–1995 | Stenni et al., 2002 |
| Adelie Land | 884 | 218 ± 69 | 1946–2006 | Goursaud et al., 2017 |
| Law Dome | 1855 | 688 | 22 BCE to 2012 | Roberts et al., 2015 |
| Aurora Basin North | 1713 | 119 | 1979–2013 | Servettaz et al., 2020 |
| Mount Brown South | 2648 | 263 ± 46 | 1979–2016 | Jackson et al., 2023 |

https://doi.org/10.5194/egusphere-2025-2408
Preprint. Discussion started: 17 July 2025


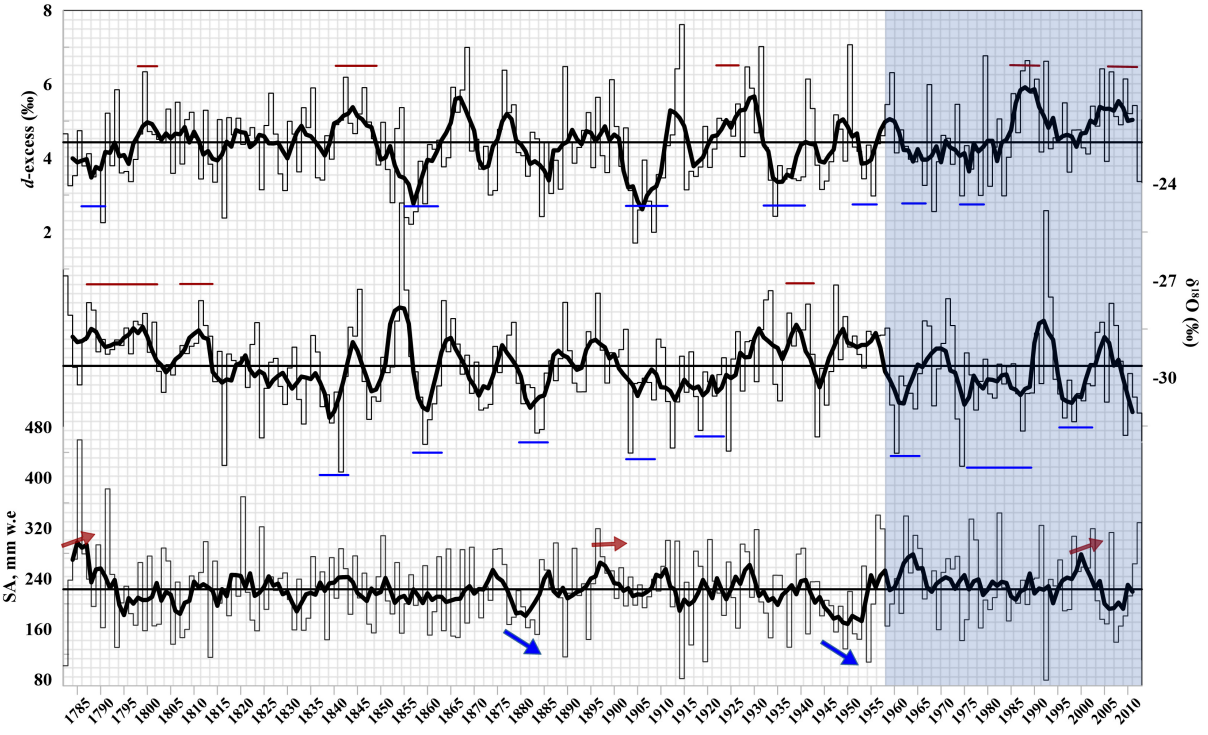


**Figure 2.** Temporal variation in the SA (bottom panel), $\delta^{18}O$ (middle panel), and *d*-excess (top panel), with the horizontal black line indicating the overall mean. The thick black lines represent the 5-year running average. The blue and red lines (arrows) indicate the periods that are higher or lower than average for at least four continuous years.

https://doi.org/10.5194/egusphere-2025-2408
Preprint. Discussion started: 17 July 2025


### 3.2 Relationship with climate variables during 1957–2013

#### 3.2.1 Relationship with climate variables from ERA5 Reanalysis

Correlation analysis was conducted on the annual means of $\delta^{18}O$, *d*-excess, and SA from the GV7-C ice core with ERA5 reanalysis data over the 1957–2013 CE period. The analysis considered climate variables on both an annual and a seasonal scale and across different pressure levels to identify any potential relationships with the GV7-C ice core data. The results are summarized in Table 5 and selectively presented in Figs. S1–S8.

The annual mean of $\delta^{18}O$ had generally positive correlations with the air temperature, SST, total precipitable water, and GPH changes, while negative correlations were observed with the SIC and wind speed (Figs. S1–S3 and Table 5). The correlations were predominantly observed during the austral summer (DJF) and autumn (MAM) seasons. While during spring (SON) season, $\delta^{18}O$ shows a negative relationship to temperature (2 m, 500 hPa, and 850 hPa) (not all shown) and total precipitable water in the inland Antarctic plateau and the IO sector. This negative relevance may indicate the isotopically differed air mass intrusion during this season. Positive correlations ($r = 0.4$, $p < 0.05$) between $\delta^{18}O$ and temperature (at 2 m and 850 hPa) and total precipitable water (Fig. S2a) were preferentially observed during the DJF season. This suggests a moisture supply from the PO (the Ross Sea) and IO sectors of the Southern Ocean (Fig. S1d–f). This is consistent with back–trajectory result for DJF season (Caiazzo et al., 2017). Indeed, the thermodynamic effect on $\delta^{18}O$ is particularly significant during the ice-free DJF season, and snowfall is large (Delmotte et al., 2000; Caiazzo et al., 2017). The influence of the wind speed and direction on $\delta^{18}O$ was observable during the DJF and MAM seasons. The belt of strong westerly winds was negatively correlated with $\delta^{18}O$ (Fig. S3). Notably, the meridional wind component (v-wind) exhibited a northward flow from the IO sector (the positive shading in Fig. S3c, f) and a southward flow from the western PO sector (negative shading in Fig. S3c, f) during the DJF season. This suggests a relatively dominant influence of the air mass from the PO sector on the $\delta^{18}O$ signal. As a result, the $\delta^{18}O$ signal in the GV7-C ice core tended to preserve the local and regional climatic conditions, particularly over the PO sector during the DJF and MAM seasons.

The annual mean value of *d*-excess exhibited a positive correlation ($0.3 < r < 0.4$, $p < 0.05$) with the air temperature (at 2 m and 850 hPa), particularly over the western PO and IO sectors (Fig. S4). Notably, significant correlations in the IO sector were evident for temperature (2 m and 850 hPa) during the SON season and on an annual scale (Figs. S4a, b, e, f), while the *d*-excess signal was weaker for changes in temperature during the DJF season. Caiazzo et al. (2017) reported dominant air mass pathways from the IO at this site based on trajectories from 2007 to 2012 CE. The results of the present study also revealed spatial correlations in the IO sector based on variation in *d*-excess over the extended period from 1957 to 2013 CE. Furthermore, the correlations with SST, SIC, and total column precipitable water supported the intrusion of air masses from the IO sector and the western PO (Fig. S5). The impact of the wind speed and wind direction on *d*-excess was relatively weak, except for the observed positive correlation with the 10-m wind speed (Figs. S6a, b). Southward flow from the IO sector and northward flow in the western PO sector (the negative and positive shading, respectively, in Fig. S6d) were also observed. Overall, this weak evidence and the absence of correlations with atmospheric circulation (i.e., dynamic effects) suggest that temperature

https://doi.org/10.5194/egusphere-2025-2408
Preprint. Discussion started: 17 July 2025


changes (i.e., thermodynamic effects) are more important for the *d*-excess observed in the GV7 ice core (Figs. S4 and S5). Unlike $\delta^{18}O$, the *d*-excess in the GV7-C ice core had seasonally consistent correlations with air temperature, indicating that the signal intensity and preservation efficiency of *d*-excess are potentially suitable for studying past oceanic climate conditions. Notably, the contribution of the air mass during the SON season may be significant for the *d*-excess signal in the GV7-C ice core.

There were no clear relationships between SA and the climate variables (Figs. S7 and S8). An exception to this was only the positive correlation between SA and the 850-hPa GPH offshore of the Ross Sea region during the MAM season (Fig. S7e). The meridional wind components (10 m and 850 hPa) indicated southward flow from this region (Fig. S8c, f), while the zonal wind components exhibited eastward flow in the Ross Sea region (Fig. S8b, e). These features suggest that the SA in the GV7-C ice core may weakly represent moisture transport from the PO sector (offshore of the Ross Sea) during the MAM season.

Collectively, the results from the spatial correlation analysis suggest that the GV7-C ice core can be used to represent the regional climate conditions over the PO and IO sector. The correlations observed with $\delta^{18}O$ during the DJF and MAM seasons led us to consider the potential influence of the SAM. It is conceivable that a positive phase of SAM during the DJF and MAM seasons could strengthen the climate signals, allowing SAM-related signals to be detectable in $\delta^{18}O$ and SA during the 1957–2013 CE period. The dynamic influence of SAM can thus be important for $\delta^{18}O$ and SA, while *d*-excess is likely to represent thermodynamic changes over the IO and western PO sectors, particularly during the SON season. These correlations for *d*-excess can be remotely connected to the temperature variability over the tropical IO and PO (Masson-Delmotte et al., 2003).

https://doi.org/10.5194/egusphere-2025-2408
Preprint. Discussion started: 17 July 2025


**Table 5.** Summary of observed correlations between the GV7-C ice core and the climate variables from the ERA5 reanalysis data by period (annual [ANN] and the DJF, MAM, JJA, and SON seasons) for the period 1957–2013 CE.

| Variables | | $\delta^{18}O$ | *d*-excess | SA |
|---|---|---|---|---|
| Air temperature | 2 m | ANN, DJF, MAM | ANN, JJA, SON, DJF | MAM |
| | 850 hPa | DJF | ANN, SON, MAM, DJF | MAM |
| SST | | ANN, MAM | SON, DJF | ANN |
| SIC | | ANN | JJA | MAM, JJA |
| Total precipitable water column | | DJF, MAM | ANN, JJA, SON, MAM | DJF, MAM |
| Geopotential height (GPH) | | DJF, MAM, SON | - | MAM |
| Wind speed | | DJF, MAM | ANN, SON | MAM |
| u-wind | | DJF, MAM | - | MAM |
| v-wind | | DJF, SON | ANN, MAM | MAM |

https://doi.org/10.5194/egusphere-2025-2408
Preprint. Discussion started: 17 July 2025


### 3.2.2 Relationship with large-scale climate modes

The SAM and ENSO are assumed to be factors that potentially affect the Antarctic climate (Turner et al., 2009). For this reason, SAM, Nino3.4, SOI indices were compared with the ERA5 reanalysis data and the GV7-C ice core records. Fig. S9 presents selectively the comparison between the SAM index and the ERA5 reanalysis data for 1979–2020 CE. Negative correlations were observed between the SAM and air temperature, SST, and moisture content, and positive correlations were present with the wind speed and SIC (not all shown in Fig. S9). Strong correlations between the SAM and climate variables were particularly evident during the DJF and MAM seasons. Meridional wind (v-wind) had a negative correlation (indicating southward flow) with the SAM over the western PO and IO sectors, suggesting dominant air mass intrusion from these sectors (Figs. S9c, f, h), while positive correlations (northward flow) were observed in the central PO sector. During the SON season, negative correlations between the 2-m temperature variability and the SAM were observed over wider coastal and oceanic temperatures over the Amundsen and Ross Sea sectors. However, this correlation over the IO sector weakened (indicated by the absence of deep negative shading), with observations confined to narrow coastal areas of East Antarctica.

The SOI and Niño3.4 indices describe changes in the PO that affect the climate over the Southern Ocean and Antarctic continent (Meyerson et al., 2002, Bertler et al., 2004). Correlation analysis between the SOI index and ERA5 reanalysis data for 1951–2020 revealed that warming over the central PO (i.e., a negative SOI) was linked to warming (i.e., the 2 m, 500 hPa, and 850 hPa temperatures) over the southern PO sector of Antarctica (data not shown). This teleconnection in the southern PO sector persisted across all seasons, with a particularly strong correlation during SON. The Niño3.4 index was compared with ERA5 reanalysis for 1940–2019 CE, with the results presented in Fig. S10. Changes in Niño3.4 were shown to be related to temperature variability (temperatures at 2 m, 850 hPa, and 500 hPa, and the SST) over the southern PO and the IO sector. Changes in the amount of moisture (i.e., total precipitation, total column precipitable water, 850 hPa GPH, and 500 hPa GPH) over the Southern Ocean were also linked to Niño3.4, with correlations observed in both the PO and IO sectors, most notably during the SON, MAM, and JJA seasons. These results suggest a potential transport mechanism via large-scale circulation or the teleconnection of tropical oceanic conditions to the Southern Ocean.

Based on the previous results, the GV7-C ice core data were compared with the SAM, Niño3.4, SOI, IOD, and SIE. PCA conducted for 1957–2013 CE, with the loading matrix presented in Table 6. Principal component (PC) 1 clustered $\delta^{18}O$, the SAM, SOI, Niño3.4, and SIE over the East Antarctica and Ross-Amundsen Sea region. This reflected the importance of both thermodynamic and dynamic effects on the decrease in $\delta^{18}O$ with an increase in the SIE, stronger westerly winds (i.e., the SAM and SOI), and lower SSTs in the Niño3.4 region. SA was associated with PC 2, with similar climate variables and the IOD, and with the lower loading for SIE in the Ross-Amundsen Sea region. This can represent the importance of dynamic effects on SA with enhanced moisture transport with strong westerlies (i.e., the SAM), increased evaporation with warm SSTs over the IO (western equatorial IO) and central tropical PO (i.e., the SOI and Niño3.4), and the wind-induced SIE over East Antarctica. The lower loading for SIE (Ross-Amundsen) implies that while the changes in SIE may be influenced by the conditions associated with IOD and SAM, this influence is relatively minor in the context of this PCA analysis. The variations

https://doi.org/10.5194/egusphere-2025-2408
Preprint. Discussion started: 17 July 2025


in SIE could be due to multiple factors, with IOD and SAM being contributors but not the dominant factors. Compared to PC1, SIE (Ross-Amundsen) has a weak relationship with IOD and SAM. PC 3 included only the GV7-C ice core records, with an increase in $\delta^{18}O$ and *d*-excess and a decrease in SA. This can be explained by the intrusion of dry-local air masses (i.e., a low SA) with evident *d*-excess signals together with $\delta^{18}O$. PC 4 was characterized by an increasing $\delta^{18}O$, *d*-excess, and SA with cooling over the southeastern equatorial IO and decrease in the SIE over East Antarctica. This may be related to changes in the intrusion from the IO sector.

The standardized values for $\delta^{18}O$, *d*-excess, and SA for 1957–2013 CE are presented with the climate variables in Figure 3. Pearson's correlation coefficients (r) for three- and five-year averages and the running-averaged and summarized in Table 7. Similar results were observed, and the correlations based on the running-averaged time series are further discussed below. The three-point running-averaged *d*-excess remained generally flat before starting to increase in 1983, while the $\delta^{18}O$ exhibited three periods of higher values (1964–1971 CE, 1989–1993 CE, and 2001–2007 CE). SA shows negative correlation only with SST-SEIO (Table 7). While the $\delta^{18}O$ (three-year running averaged time series) exhibited moderate positive ($r = 0.46$, $p < 0.001$, $n = 54$) and negative ($r = -0.49$, $p < 0.001$, $n = 54$) correlations with Niño3.4 and SOI, respectively. There was also a weak correlation ($r = -0.32$, $p < 0.05$, $n = 54$) with the SIE over the Ross-Amundsen Sea region. For *d*-excess (e.g., three-year smoothed time series), moderate positive correlation observed with SST-SEIO ($r = 0.72$, $p < 0.001$ $n = 54$). Interestingly, *d*-excess had no correlation with the IOD index (SST gradient between the tropical western and southeastern Indian Ocean) during 1957–2013 CE period. Moreover, weak positive correlations were observed in the five-year smoothed time series with the SAM ($r = 0.37$, $p < 0.005$, $n = 52$), Niño 3.4 ($r = 0.32$, $p < 0.05$, $n = 52$), and SIE over the Ross-Amundsen Sea ($r = 0.47$, $p < 0.001$, $n = 52$). The correlation coefficients tended to increase for *d*-excess as the smoothing increased. These results likely to suggest that variation in $\delta^{18}O$ and *d*-excess captures climatic signals for the 1957–2013 CE period, particularly over southern sector of the PO as well as the southeastern IO.

https://doi.org/10.5194/egusphere-2025-2408
Preprint. Discussion started: 17 July 2025


280

**Table 6.** Loadings of the variables for the first four principal components (PCs) of the PCA analysis conducted with the data for 1957–2013 CE. Larger values (r > 0.3) are marked in bold.

| Variables | PC1 | PC2 | PC3 | PC4 |
|---|---|---|---|---|
| SA | 0.03 | **0.36** | **–0.57** | **0.54** |
| $\delta^{18}O$ | **–0.40** | –0.01 | **0.57** | **0.33** |
| *d*-excess | 0.06 | 0.01 | **0.74** | **0.45** |
| IOD | 0.11 | **0.72** | –0.21 | **0.32** |
| SAM | **0.53** | **0.60** | 0.16 | –0.18 |
| SOI | **0.81** | **–0.46** | –0.11 | 0.22 |
| Niño3.4 | **–0.79** | **0.50** | 0.11 | –0.14 |
| SIE (East Antarctica) | **0.53** | **0.42** | 0.26 | **–0.38** |
| SIE (Ross-Amundsen Sea) | **0.85** | 0.17 | 0.20 | 0.08 |
| *Variance explained (%)* | *30* | *19* | *16* | *10* |
| *Cumulative percent (%)* | *30* | *49* | *65* | *75* |

https://doi.org/10.5194/egusphere-2025-2408
Preprint. Discussion started: 17 July 2025


**Table 7.** Pearson's correlation coefficients (r) between the three- and five-year average (in parentheses) and running averaged time series of the GV7-C ice core records and the climate variables for the period 1957–2013 CE. Larger values ($r > 0.3$ at $p < 0.05$) are marked in bold. SIE (EA) and SIE (RA) denotes sea ice extent over East Antarctica and the Ross-Amundsen Sea sector.

| | IOD | SST (SEIO) | SAM | SOI | Niño3.4 | SIE (EA) | SIE (RA) |
|---|---|---|---|---|---|---|---|
| | | | | 3-yr mean | | | |
| SA | 0.18 (0.12) | **–0.36 (–0.52)** | –0.06 (–0.13) | 0.09 (–0.04) | –0.14 (0.08) | 0.04 (0.19) | –0.02 (–0.22) |
| $\delta^{18}O$ | –0.02 (–0.26) | 0.04 (0.14) | –0.27 **(–0.43)** | **–0.49 (–0.54)** | **0.46 (0.43)** | –0.11 (–0.27) | **–0.32 (–0.33)** |
| *d*-excess | –0.06 (–0.18) | **0.72 (0.81)** | 0.21 (0.19) | –0.09 (–0.16) | 0.27 (0.18) | –0.16 (–0.21) | **0.31 (0.30)** |
| | | | | 5-yr mean | | | |
| SA | –0.10 (–0.06) | **–0.42 (–0.40)** | –0.11 (–0.16) | 0.10 (–0.08) | –0.20 (0.13) | –0.03 (–0.28) | –0.15 (–0.16) |
| $\delta^{18}O$ | 0.00 (–0.24) | 0.11 (–0.13) | –0.25 **(–0.39)** | **–0.44 (–0.42)** | **0.49 (0.37)** | –0.15 **(–0.41)** | –0.27 (–0.29) |
| *d*-excess | 0.08 (0.01) | **0.79 (0.70)** | **0.37** (0.20) | –0.13 (–0.25) | **0.32** (0.29) | –0.12 (–0.22) | **0.47** (0.27) |

https://doi.org/10.5194/egusphere-2025-2408
Preprint. Discussion started: 17 July 2025


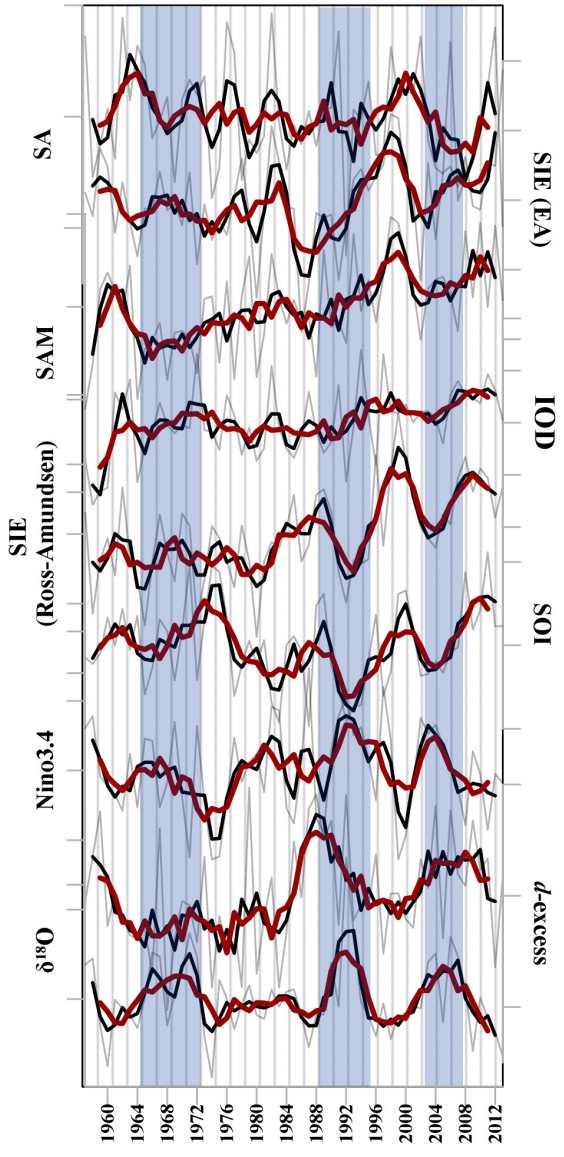


290 **Figure 3.** Comparison of the standardized profiles (grey lines) for SA, $\delta^{18}O$, and *d*-excess with the climate variables for 1957–2013 CE. The red and blue lines indicate the 3- and 5-year running average. The vertical red shading indicates periods with large $\delta^{18}O$ values.

https://doi.org/10.5194/egusphere-2025-2408
Preprint. Discussion started: 17 July 2025


### 3.3 Relationship with Long-Term Climate Modes

The GV7-C ice core data were also compared with long-term records (1872–2013 CE) for the SAM, Niño3.4, IOD, SST-SEIO, and SST anomaly over the Southern Hemisphere (Fig. 4 and Table 8). Pearson's correlation coefficients (r) for three-year and five-year averages, along with the running-averaged data, are shown in Table 8. The correlations on the running-averaged data are discussed below. The running average time series for *d*-excess (five-year) was correlated with the IOD ($r = 0.3$, $n = 138$, $p < 0.001$), SST-SEIO ($r = 0.46$, $n = 138$, $p < 0.001$), SAM ($r = 0.3$, $n = 138$, $p < 0.001$), and SST anomalies over the Southern Hemisphere ($r = 0.43$, $n = 138$, $p < 0.001$) (Table 8 and Fig. 4). There was no clear relevance between *d*-excess and Niño3.4 index. Notably, *d*-excess had no correlation with the IOD for 1957–2013 CE (Table 7) but did so for 1872–2013 CE as well as with the SST-SEIO. The spatial correlation of *d*-excess with the reconstructed SST dataset was also tested for three periods: 1979–2013 CE, 1957–2013 CE, and 1854–2013 CE (Fig. 5). Notably, *d*-excess exhibited no correlations during the 1979–2013 CE period (Fig. 5a) as well as 1979-1999 CE and 1999–2013 CE (not shown), while weak positive correlations were observed over the remote IO sector during the 1957–2013 CE period (Fig. 5b). In the period from 1854 to 2013 CE, a weak positive correlation was observed over a larger area in the southern sector of the IO (Fig. 5c). Consistently large peaks in the five-year running averaged time series for *d*-excess (both high and low values) were more frequent after 1845 (Fig. 4). Furthermore, it can be reported that the increasing phases in the global average temperature during the 1910–1945 CE period and since 1976 (IPCC, 2001) are evident in the increasing trend for *d*-excess (Fig. 4). The *d*-excess signal from the GV7-C ice core can be roughly suggested to representing thermodynamic changes (i.e., SST changes) over the IO sector of the Southern Ocean, at least over the 1872–2013 CE period. However, the *d*-excess signal can be affected when the SAM changes.

In the long-term analysis, correlations of $\delta^{18}O$ and SA with the climate variables disappeared, suggesting the signal intensity may have been smoothed due to various influencing factors. However, some evident relevance can still be observed in the short-term period for $\delta^{18}O$ and SA. The decrease in SA during the 1876–1885 CE and 1940–1955 CE periods was consistent with the increasing trend in the SAM, indicating the presence of cold and windy conditions during these periods. Considering the correlation of $\delta^{18}O$ with Niño3.4 ($r = 0.49$) and SOI ($r = -0.44$) for 1957–2013 CE (Table 7), this suggests the influence of SST changes in the PO sector. However, this correlation weakened over a longer period (1872–2013). The recent trend (1985–2013) for $\delta^{18}O$ was also found to be in line with Niño3.4 and the SAM index (Fig. 4). The variation in the SAM observed during the recent period is unprecedented in the last millennia (Fogt and Marshall, 2020). The increasing influence of the SAM-ENSO coupling has been reported since the 1940s in coastal Dronning Maud Land (Ejaz et al., 2022). It can then be assumed that the trends towards a more positive phase of SAM in recent decades has led increasing cyclones in the Southern Ocean that has increased transport efficiency from multiple air masses or increased the contribution of local transport from the PO sector. Conversely, the negative SAM in the period before the 1980s may have weakened the signals from the PO sector, with the signals from the main air mass source region (i.e., the IO sector) becoming more evident.

https://doi.org/10.5194/egusphere-2025-2408
Preprint. Discussion started: 17 July 2025


**Table 8.** Pearson's correlation coefficients between the three- and five-year average (in parentheses) and running averaged time series of the GV7-C ice core records and the climate variables for the period 1872–2013 CE. Larger values ($r > 0.3$ at $p < 0.05$) are marked in bold.

| | IOD | SST (SEIO) | SST anomaly | SAM | Niño3.4 |
|---|---|---|---|---|---|
| | | | 3-yr mean | | |
| SA | 0.01 (–0.07) | 0.02 (–0.01) | 0.02 (–0.06) | 0.09 (–0.02) | 0.03 (0.07) |
| $\delta^{18}O$ | –0.11 (–0.16) | –0.02 (–0.17) | –0.11 (–0.20) | –0.22 (–0.19) | 0.18 (0.18) |
| *d*-excess | 0.23 (0.29) | **0.43 (0.41)** | **0.39 (0.40)** | 0.28 (0.25) | 0.26 **(0.35)** |
| | | | 5-yr mean | | |
| SA | –0.04 (–0.08) | 0.11 (0.05) | 0.04 (0.00) | 0.07 (0.08) | 0.15 (–0.01) |
| $\delta^{18}O$ | –0.09 (–0.21) | –0.03 (–0.21) | –0.11 (–0.26) | –0.14 (–0.21) | 0.12 (0.04) |
| *d*-excess | **0.30 (0.31)** | **0.46 (0.44)** | **0.43 (0.39)** | **0.30** (0.22) | 0.16 (0.27) |

https://doi.org/10.5194/egusphere-2025-2408
Preprint. Discussion started: 17 July 2025


330

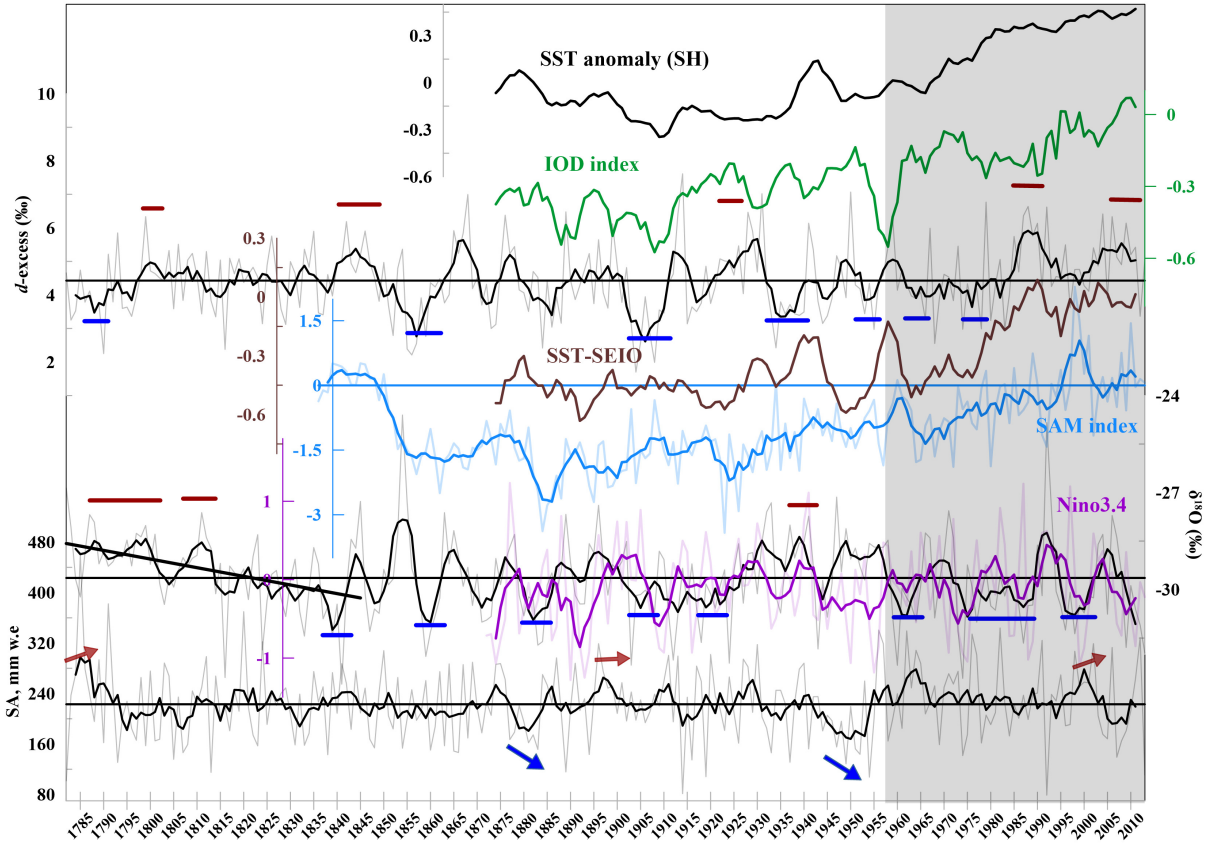


**Figure 4.** Comparison of the 5-year running average for SA, $\delta^{18}O$, and *d*-excess with the IOD, SST anomaly of the southeastern Indian Ocean (SST-SEIO), SST anomalies over the Southern Hemisphere, the SAM, and Nino3.4 for 1872–2013 CE. The SAM index is presented with the annual mean (thin blue line) and the neutral (at zero) horizontal line. The thin purple line indicates the annual mean of Nino3.4. The thin grey line represents the annual mean of the SA, $\delta^{18}O$, and *d*-excess. The blue and red lines (or arrows) indicate the periods with a higher or lower than average SA, $\delta^{18}O$, and *d*-excess over at least four consecutive years. The gray shading corresponds to the period after 1957. The linear trend in $\delta^{18}O$ during the 1782–1845 CE period is represented by the black line.

https://doi.org/10.5194/egusphere-2025-2408
Preprint. Discussion started: 17 July 2025


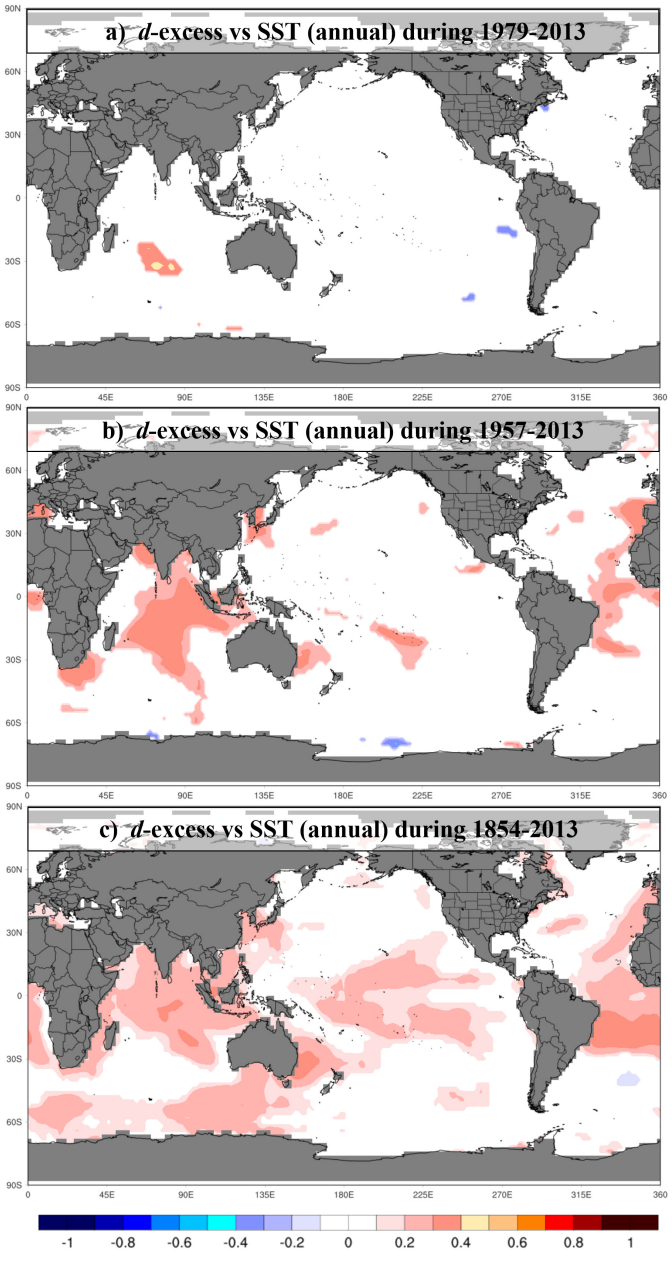


**Figure. 5.** Spatial correlation of *d*-excess with annual SST variability for (a) 1979–2013 CE, (b) 1957–2013 CE, and (c) 1854–2013 CE. The scale bars indicate Pearson's correlation coefficient (r) at $p < 0.05$. This figure was generated using Climate Reanalyzer (https://climatereanalyzer.org/) from the Climate Change Institute, University of Maine, USA.

https://doi.org/10.5194/egusphere-2025-2408
Preprint. Discussion started: 17 July 2025


## 4 Discussion and implications

Based on the correlation of $\delta^{18}O$ in the GV7-C ice core with Nino 3.4, SOI, SAM, and SIE over the Ross-Amundsen Sea sector for 1957–2013 CE, the increasing (decreasing) $\delta^{18}O$ can be explained by the intrusion of relatively warm (colder) and moist (dry) air mass mainly through the PO sector of the Southern Ocean. This finding is comparable to other ice cores from the coastal Antarctica. In the Aurora Basin North ice core from East Antarctica, a weak negative correlation (r = –0.24) was observed between the SAM and $\delta^{18}O$ for 2005–2014 CE (Servettaz et al., 2020). This suggests a negative phase of the SAM channeled the intrusion of warm and moist air inland, consequently causing an increase in $\delta^{18}O$ at this site. Large precipitation events on the East Antarctic Plateau were associated to high pressure over northeast of Aurora Basin North drilling site, based on the 500-hPa GPH and mean 2-m temperature anomaly data for the period 1979–2015 CE. Further evidence for moisture transport from the southern IO has been found in the Mount Brown South ice core (facing the IO sector of the Southern Ocean) in East Antarctica (Jackson et al., 2023). This study also suggests the precipitation events are linked with high-pressure systems in the mid-latitudes which increase the transport of warm and moist air mass from the southern IO. In another ice core from Adélie Land covering the 1946–2006 CE period, decadal variations in $\delta^{18}O$ and regional temperature were correlated (Goursaud et al., 2017). Moreover, $\delta^{18}O$ shows a tendency to decrease with increasing wind speed. However, the $\delta^{18}O$ on an annual scale could not be explained by changes in the SIE and temperature, indicating the importance of site-dependent climate signals in coastal ice cores (Goursaud et al., 2017). In another study, Bertler et al. (2011) reported colder SSTs, a higher SIE, stronger katabatic winds, and decreasing SA in the Victoria Low Glacier ice core during the 1288–1807 period, which was identified as the Little Ice Age period. Little Ice Age-related cooling is also evident in the $\delta^{18}O$ signal from the Hercules Neve ice core for the 1770–1890 period (Stenni et al., 1999) and frequent cold intervals in the Talos Dome ice core (Stenni et al., 2002). In line with these observations, a slight decreasing trend was observed in the $\delta^{18}O$ signal from the GV7-C ice core during the 1782–1845 CE period (Fig. 4), which may be part of Little Ice Age cooling. After 1845, there was no long-term trend in $\delta^{18}O$ from the GV7-C ice core; rather, values lower than the long-term mean were frequently observed (the blue lines in Fig. 4). This depletion of $\delta^{18}O$ observed from the GV7-C ice core may be possibly linked with changes in atmospheric circulation (e.g., SAM-related cooling) (Thompson and Solomon, 2002). Moreover, in terms of temperature reconstruction, $\delta^{18}O$ signal in the GV7-C ice core is contrast to anthropogenic global warming, suggesting more local/regional variations or various climatic factors.

It is known that *d*-excess is an indicator of climate conditions in the evaporation source region (Jouzel et al., 1982; Sodemann and Stohl, 2009, Lewis et al., 2013). Warming over the Southern Ocean, except the Atlantic sector, was found to co-vary with higher *d*-excess in the Victoria Lower Glacier ice core during the 1991–2000 CE period (Bertler et al., 2011). At the Law Dome ice core site, *d*-excess also reflects SST changes over the southern IO sector (Masson-Delmotte et al., 2003). Particularly the abrupt increase in the *d*-excess in the 1970s was consistent with the GV7-C ice core result. This relevance was explained by the abrupt changes in meridional atmospheric circulation, which led to the intrusion of warm subtropical moisture sources to the Antarctic coast during the 1970s (Masson-Delmotte et al., 2003). Changes in the SAM have also been linked to tropical

https://doi.org/10.5194/egusphere-2025-2408
Preprint. Discussion started: 17 July 2025


SST changes and other tropical variabilities (Clem and Fogt, 2013; Ding et al., 2012). The climate signals in some coastal sites, including RICE, Mt. Erebus Saddle, and Styx Glacier, have been thought to be primarily indicative of local and regional conditions in the Ross Sea region (Rhodes et al., 2012, Nyamgerel et al., 2020, 2024). In the GV7-C ice core site, variabilities linked to the SAM and remote teleconnections with SST over the IO sector of the Southern Ocean were assumed to be associated with *d*-excess. The influence IOD on the eastern East Antarctic precipitation was more dominant than the SAM-induced changes for the 1979–2014 (Lee and Jin, 2024). The IOD-related variation in the precipitation is explained by waves originating from the Indian Ocean that propagate southeastward, and inducing a low-pressure anomaly near eastern east Antarctica, consequently reducing precipitation.

Based on various correlation analysis with the climate variables used in this study for the periods 1957–2013 CE and 1872–2013 CE, the following interpretations are summarized. During the period 1957–2013 CE, the correlation patterns based on $\delta^{18}O$ and *d*-excess support that snow precipitating at the GV7-C site mainly originates from the Southern Ocean possibly via western PO and the Indian Ocean sector (southeastern Indian Ocean). For the longer time scale (1872–2013), the correlation patterns based on *d*-excess for SST indicates air mass from the Southern Ocean possibly via the Indian Ocean sector. This suggests a warmer (colder) ocean surface condition would be preserved in higher (lower) $\delta^{18}O$ (recent period) and *d*-excess values (recent and longer period) in the GV7-C ice core. Overall, the relevance between ice core records and climate variables is sensitive to the averaging of the time series, the climatology of specific seasons, and the time period under consideration. Influence of atmospheric circulation, transport efficiency, and abrupt synoptic events needs to be considered for the interpretation of Antarctic ice core data.

The SA variability in the GV7-C ice core exhibited no consistent trend, which may be due to multiple influencing factors, including non-climatic noise. In the Talos Dome ice core, the water isotopic and SA records indicated the influence of warm-air intrusion and wind patterns close to the ice divide between Oates Land and the Ross Sea (Stenni et al., 2002). Roberts et al. (2015) identified the influence of the ENSO on SA at the Law Dome site. Thermodynamic processes attributed to changes in the air temperature (e.g., wind or relative humidity) lead to an increase in the moisture content and thus a higher SA over Antarctica (Medley and Thomas, 2019). Moreover, moisture transport via large-scale atmospheric circulation (Thomas et al., 2008) and synoptic-scale short-lived events (e.g., atmospheric river events) influences interannual variability in SA (Turner et al., 2019) and evident in the ice core records from coastal regions (Servettaz et al., 2020; Jackson et al., 2023). The intensity and frequency of cyclone events also affect snowfall in Antarctic coastal areas (Dalaiden et al., 2020a). Cyclonically driven SA is known to be dominant in the Ross Sea region and sensitive to tropical and local climate drivers (Bertler et al., 2018). The contribution of synoptic-scale transport has been estimated to be large for Victoria Land based on simulations over the 1985–2014 period (Dalaiden et al., 2020a). The variations in SA data from the GV7-C ice core show no obvious trend and are not correlated to climate drivers examined in this study. The SA of the GV7-C ice core is assumed to be affected by the coupled influence of dynamic processes (i.e., the transport pathways and transport efficiency of moist air) or abrupt synoptic events (e.g., intense transport by atmospheric river events).

https://doi.org/10.5194/egusphere-2025-2408
Preprint. Discussion started: 17 July 2025


It is useful for interpreting extended ice core records that cover known climatic periods. In the context of global warming scenarios, understanding the historical temperature variability over the tropical ocean is important (IPCC, 2019). Heat transported by the Southern Ocean induces the melting of Antarctic ice shelves (Rignot et al., 2019), and the projections over the next century show oceanic and atmospheric warming (Timmermann and Hellmer, 2013). Particularly, the Indian Ocean is experiencing the strongest and most robust warming signal of the global oceans (Du and Xie, 2008; Beal et al., 2019), largely driven by anthropogenic forcing (Dong et al., 2014), and it is projected to warm non-uniformly (Sharma et al., 2023). The variations in the IO and the PO temperature anomaly affect the surface air temperature of Antarctica (Zhang and Duan, 2023). Warm SSTs in the western tropical IO excite a poleward-moving Rossby wave, inducing the loss of sea ice in the Amundsen Sea and an increase in other coastal regions during the 1979–2020 CE period (Zhang et al., 2024). The coastal and inland Antarctic regions emerge an anomalous retreat of sea ice extent and warming due to the short-term significant intrusion of warm and moist air masses associated with strong negative phase of SAM (Ionita et al., 2018). Thus, understanding the response of the Antarctic climate to ocean variability of the IO sector would be important. The results of this study may be useful for understanding ocean–atmosphere feedback between tropical oceans and the high-latitude Southern Ocean.

## 5 Conclusions

$\delta^{18}O$, *d*-excess, and SA data from the GV7-C ice core in East Antarctica for the 1782–2014 CE period were studied to identify potential correlations with various climate variables at different temporal resolutions (1957–2013 CE and 1872–2013 CE). Snow accumulation data from the GV7-C ice core were not strongly correlated with climate variables, while $\delta^{18}O$ and *d*-excess exhibited correlations with climate indices representing changes in the Pacific (Niño3.4, SOI, and SIE in the Ross-Amundsen Sea sector) and in the Indian Ocean sector (SST-SEIO) of the Southern Ocean during the 1957–2013 CE period. The SAM was also correlated with *d*-excess during this period. In the long-term analysis (1872–2013 CE), the correlation of $\delta^{18}O$ with the climate variables disappeared, suggesting a shift in the dominant climatic factors. In contrast, *d*-excess maintained its weak correlation with the SAM, while also exhibiting correlations with the IOD, SST-SEIO, and SST over the Southern Hemisphere. Based on various correlation analysis with the climate variables used in this study, during 1957–2013 CE, correlation patterns based on $\delta^{18}O$ and *d*-excess suggest that snow at the GV7-C site originates from the Southern Ocean, possibly via the western Pacific and southeastern Indian Ocean. For 1872–2013 CE, *d*-excess and SST correlations indicate the Southern Ocean origin, likely through the Indian Ocean sector. Overall, this study provides potential insights into teleconnections with low-latitude climate, possibly over the Indian Ocean sector of the Southern Ocean, which is important in the context of global warming. Efforts to capture potential climatic signals in the GV7-C ice record may be sensitive to the resolution of the time series and the use of different time periods.

https://doi.org/10.5194/egusphere-2025-2408
Preprint. Discussion started: 17 July 2025


**Code and data availability.** Data reported in this study have been deposited at the Korea Polar Data Center (KPDC). Stable water isotope composition of the shallow ice core drilled at the GV7 site in 2013-2014. Dating the ice core/Paleoclimate research (https://dx.doi.org/doi:10.22663/KOPRI-KPDC-00000654). Climate Reanalyzer (https://climatereanalyzer.org/) from the Climate Change Institute, University of Maine, US, is publicly available.

**Author contributions.** YN: Conceptualization, Data analysis, Writing – original draft, Review and editing. YH: Conceptualization, Data analysis, Review and editing. SDH: Conceptualization, Review and editing. HK: Conceptualization, Review and editing. SK: Data analysis, Review and editing, JM: Data analysis, Review and editing, BS: Conceptualization, Review and editing, JL: Conceptualization, Review and editing.

**Competing interests.** The authors declare that they have no conflict of interest.

**Financial support.** This work was supported by a Korea Polar Research Institute grant (PE25100) and a National Research Foundation of Korea grant funded by the Korean government (2022R1A2C3007047). This work was partially supported by Korea Institute of Marine Science & Technology Promotion (KIMST) funded by the Ministry of Oceans and Fishers (RS-2023-00256677; PM23020).

https://doi.org/10.5194/egusphere-2025-2408
Preprint. Discussion started: 17 July 2025


## References

Becagli, S., Proposito, M., Benassai, S., Flora, O., Genoni, L., Gragnani, R., Largiuni, O., Pili, S.L., Severi, M., Stenni, B., Traversi, R., Udisti, R., and Frezzotti, M.: Chemical and isotopic snow variability in East Antarctica along the 2001/02 ITASE traverse. Annals of Glaciology, 39, 473–482. https://doi.org/10.3189/172756404781814636, 2004.

Beal, L.M., Vialard, J., Roxy, M.K., and lead authors.: IndOOS-2: a roadmap to sustained observations of the Indian Ocean for 2020–2030. CLIVAR-4/2019. https://doi.org/10.36071/clivar.rp.4-1.2019, 2019.

Bertler, N. A. N., Barrett, P. J., Mayewski, P. A., Fogt, R. L., Kreutz, K. J., and Shulmeister, J.: El Ni˜no suppresses Antarctic warming, Geophys. Res. Lett., 31, L15207, doi:10.1029/2004GL020749, 2004.

Bertler, N.A.N, Mayewski, P., and Carter, L.: Cold conditions in Antarctica during the Little Ice Age – implications for abrupt climate change mechanisms. Earth and Planetary Science Letters, 308, 41–51, https://doi.org/10.1016/j.epsl.2011.05.021, 2011.

Bertler, N. A. N., Conway, H., Dahl-Jensen, D., Emanuelsson, D. B., Winstrup, M., Vallelonga, P. T., Lee, J. E., Brook, E. J., Severinghaus, J. P., Fudge, T. J., Keller, E. D., Baisden, W. T., Hindmarsh, R. C. A., Neff, P. D., Blunier, T., Edwards, R., Mayewski, P. A., Kipfstuhl, S., Buizert, C., Canessa, S., Dadic, R., Kjær, H. A., Kurbatov, A., Zhang, D., Waddington, E. D., Baccolo, G., Beers, T., Brightley, H. J., Carter, L., Clemens-Sewall, D., Ciobanu, V. G., Delmonte, B., Eling, L., Ellis, A., Ganesh, S., Golledge, N. R., Haines, S., Handley, M., Hawley, R. L., Hogan, C. M., Johnson, K. M., Korotkikh, E., Lowry, D. P., Mandeno, D., McKay, R. M., Menking, J. A., Naish, T. R., Noerling, C., Ollive, A., Orsi, A., Proemse, B. C., Pyne, A. R., Pyne, R. L., Renwick, J., Scherer, R. P., Semper, S., Simonsen, M., Sneed, S. B., Steig, E. J., Tuohy, A., Venugopal, A. U., Valero-Delgado, F., Venkatesh, J., Wang, F., Wang, S., Winski, D. A., Winton, V. H. L., Whiteford, A., Xiao, C., Yang, J., and Zhang, X.: The Ross Sea dipole – temperature, snow accumulation and sea ice variability in the Ross Sea region, Antarctica, over the past 2700 years. Climate of the Past, 14, 193–214. https://doi.org/10.5194/cp-14-193-2018, 2018.

Caiazzo, L., Baccolo, G., Barbante, C., Becagli, S., Berto, M., Ciardini, V., Crotti, I., Delmonte, B., Dreossi, G., Frezzotti, M., Gabrieli, J., Giardi, F., Han, Y., Hong, S-B., Hur, S.D., Hwang, H., Kang, J-H., Narcisi, B., Proposito, M., Scarchilli, C., Selmo, E., Severi, M., Spolaor, A., Traversi, R., and Udisti, R.: Prominent features in isotopic, chemical and dust stratigraphies from coastal East Antarctic ice sheet (Eastern Wilkes Land). Chemosphere, 176, 273-287. https://doi.org/10.1016/j.chemosphere.2017.02.11, 2017.

Clem, K. R., and Fogt, R. L. Varying roles of ENSO and SAM on the Antarctic Peninsula climate in austral spring. Journal of Geophysical Research: Atmospheres, 118(20), 11,481–11,492. https://doi.org/10.1002/jgrd.50860, 2013.

Constable, A.J., Harper,S., Dawson, J., Holsman, K., Mustonen, T., Piepenburg, D., and Rost, B.: Cross-Chapter Paper 6: Polar Regions. In: Climate Change 2022: Impacts, Adaptation and Vulnerability. Contribution of Working Group II to the Sixth Assessment Report of the Intergovernmental Panel on Climate Change [H.-O. Pörtner, D.C. Roberts, M. Tignor,E.S. Poloczanska, K. Mintenbeck, A. Alegría, M. Craig, S. Langsdorf, S. Löschke, V. Möller, A. Okem, B.

https://doi.org/10.5194/egusphere-2025-2408
Preprint. Discussion started: 17 July 2025


Rama (eds.)].Cambridge University Press, Cambridge, UK and New York, NY, USA, pp. 2319–2368, doi:10.1017/9781009325844.023, 2022.

Craig, H.: Isotopic variations in meteoric waters. Science, 133, 1702–1703. DOI: 10.1126/science.133.3465.1702, 1961.

Dalaiden, Q., Goosse, H., Lenaerts, J.T.M., Cavitte, M.G.P., and Henderson, N.: Future Antarctic snow accumulation trend is dominated by atmospheric synoptic-scale events. Communications Earth & Environment, 1, 62. https://doi.org/10.1038/s43247-020-00062-x, 2020a.

Dalaiden, Q., Goosse, H., Klein, F., Lenaerts, J. T. M., Holloway, M., Sime, L., and Thomas, E.R.: How useful is snow accumulation in reconstructing surface air temperature in Antarctica? A study combining ice core records and climate models, The Cryosphere, 14, 1187–1207, https://doi.org/10.5194/tc-14-1187-2020, 2020b.

Delmotte, M., Masson, V., Jouzel J, and Morgan, V.: A seasonal deuterium excess signal at Law Dome, coastal Eastern Antarctica: a Southern Ocean signature. Journal of Geophysical Research 105(D6): 7187–7197, 2000.

Ding, Q., Steig, E. J., Battisti, D. S., and Wallace, J. M.: Influence of the tropics on the Southern Annular Mode. Journal of Climate, 25 (18), 6330–6348. https://doi.org/10.1175/JCLI-D-11-00523.1, 2012.

Divine, D. V., E. Isaksson, M. Kaczmarska, F. Godtliebsen, H. Oerter, E. Schlosser, S. J. Johnsen, M. van den Broeke, and R. S. W. van de Wal.: Tropical Pacific–high latitude south Atlantic teleconnections as seen in $\delta^{18}O$ variability in Antarctic coastal ice cores, J. Geophys. Res., 114, D11112, doi:10.1029/2008JD010475, 2009.

Dong, L., Zhou, T., and Wu, B.: Indian Ocean warming during 1958–2004 simulated by a climate system model and its mechanism. Clim Dyn 42, 203–217. https://doi.org/10.1007/s00382-013-1722-z, 2014.

Ejaz, T., Rahaman, W., Laluraj, C.M., Mahalinganathan, K., and Thamban, M.: Rapid Warming Over East Antarctica Since the 1940s Caused by Increasing Influence of El Niño Southern Oscillation and Southern Annular Mode. Front. Earth Sci. 10:799613. doi: 10.3389/feart.2022.799613, 2022.

Fogt, R. L., Wovrosh, A. J., Langen, R. A., and Simmonds, I.: The characteristic variability and connection to the underlying synoptic activity of the Amundsen-Bellingshausen Seas Low. Journal of Geophysical Research, 117, D07111. doi:10.1029/2011JD017337, 2012.

Fogt, R.L., and Marshall GJ.: The Southern Annular Mode: Variability, trends, and climate impacts across the Southern Hemisphere. WIREs Clim Change. 2020; 11:e652. https://doi.org/10.1002/wcc.652, 2020.

Fogt, R. L., Raphael, M. N., and Handcock, M.S.: Seasonal Antarctic Sea Ice Extent Reconstructions, 1905-2020, Version 1. [East Antarctica and Ross-Amundsen reconstruction ensembles]. Boulder, Colorado USA. NSIDC:National Snow and Ice Data Center. https://doi.org/10.7265/55x7-we68, 2023.

Fretwell, P., Pritchard, H. D., Vaughan, D. G., Bamber, J. L., Barrand, N. E., Bell, R., Bianchi, C., Bingham, R. G., Blankenship, D. D., Casassa, G., Catania, G., Callens, D., Conway, H., Cook, A. J., Corr, H. F. J., Damaske, D., Damm, V., Ferraccioli, F., Forsberg, R., Fujita, S., Gim, Y., Gogineni, P., Griggs, J. A., Hindmarsh, R. C. A., Holmlund, P., Holt, J. W., Jacobel, R. W., Jenkins, A., Jokat, W., Jordan, T., King, E. C., Kohler, J., Krabill, W., Riger-Kusk, M., Langley, K. A., Leitchenkov, G., Leuschen, C., Luyendyk, B. P., Matsuoka, K., Mouginot, J., Nitsche, F. O., Nogi, Y., Nost,

https://doi.org/10.5194/egusphere-2025-2408
Preprint. Discussion started: 17 July 2025


O. A., Popov, S. V., Rignot, E., Rippin, D. M., Rivera, A., Roberts, J., Ross, N., Siegert, M. J., Smith, A. M., Steinhage, D., Studinger, M., Sun, B., Tinto, B. K., Welch, B. C., Wilson, D., Young, D. A., Xiangbin, C., and Zirizzotti, A.: Bedmap2: improved ice bed, surface and thickness datasets for Antarctica, The Cryosphere, 7, 375–393, https://doi.org/10.5194/tc-7-375-2013.

Frezzotti, M., Urbini, S., Proposito, M., Scarchilli, C., and Gandolfi, S.: Spatial and temporal variability of surface mass balance near Talos Dome, East Antarctica. Journal of Geophysical Research, 112, F02032. https://doi.org/10.1029/2006JF000638, 2007.

Frieler, K., Clark, P., He, F., Buizert, C., Reese, R., Ligtenberg, S.R.M., van den Broeke, M.R., Winkelmann, R., and Levermann, A.: Consistent evidence of increasing Antarctic accumulation with warming. Nature Climate Change, 5, 348–352. https://doi.org/10.1038/nclimate2574, 2015.

Goursaud, S., Masson-Delmotte, V., Favier, V., Preunkert, S., Fily, M., Gallée, H., Jourdain, B., Legrand, M., Magand, O., Minster, B., and Werner, M.: A 60-year ice-core record of regional climate from Adélie Land, coastal Antarctica. The Cryosphere, 11, 343–362. doi: 10.5194/tc-11-343-2017, 2017.

Goursaud, S., Masson-Delmotte, V., Favier, V., Preunkert, S., Legrand, M., Minster, B., and Werner, M.: Challenges associated with the climatic interpretation of water stable isotope records from a highly resolved firn core from Adélie Land, coastal Antarctica. The Cryosphere, 13, 1297–1324. https://doi.org/10.5194/tc-13-1297-2019, 2019.

Hall, A., and Visbeck, M.: Synchronous variability in the southern hemisphere atmosphere, sea ice, and ocean resulting from the annular mode. Journal of Climate, 15: 3043–3057. https://doi.org/10.1175/1520-0442(2002)015<3043:SVITSH>2.0.CO;2, 2002.

Huang, B., Thorne, P.W., Banzon, V.F., Boyer, T., Chepurin, G., Lawrimore, J.H., Menne, M.J., Smith, T.M., Vose, R.S., and Zhang, H-M.: NOAA Extended Reconstructed Sea Surface Temperature (ERSST), Version 5. [Southern Hemisphere Ocean Temperature Anomalies]. NOAA National Centers for Environmental Information. doi:10.7289/V5T72FNM, 2017.

Ionita, M., Scholz, P., Grosfeld, K., and Treffeisen, R.: Moisture transport and Antarctic sea ice: austral spring 2016 event, Earth Syst. Dynam., 9, 939–954, https://doi.org/10.5194/esd-9-939-2018, 2018.

IPCC, 2001: Climate Change 2001: The Scientific Basis. Contribution of Working Group I to the Third Assessment Report of the Intergovernmental Panel on Climate Change [Houghton, J.T.,Y. Ding, D.J. Griggs, M. Noguer, P.J. van der Linden, X. Dai, K. Maskell, and C.A. Johnson (eds.)]. Cambridge University Press, Cambridge, United Kingdom and New York, NY, USA, 881pp.

IPCC, 2019: Technical Summary [H.-O. Pörtner, D.C. Roberts, V. Masson-Delmotte, P. Zhai, E. Poloczanska, K. Mintenbeck, M. Tignor, A. Alegría, M. Nicolai, A. Okem, J. Petzold, B. Rama, N.M. Weyer (eds.)]. In: IPCC Special Report on the Ocean and Cryosphere in a Changing Climate [H.- O. Pörtner, D.C. Roberts, V. Masson-Delmotte, P. Zhai, M. Tignor, E. Poloczanska, K. Mintenbeck, A. Alegría, M. Nicolai, A. Okem, J. Petzold, B. Rama, N.M. Weyer (eds.)]. In press.

https://doi.org/10.5194/egusphere-2025-2408
Preprint. Discussion started: 17 July 2025


Jackson, S. L., Vance, T. R., Crockart, C., Moy, A., Plummer, C., and Abram, N. J.: Climatology of the Mount Brown South ice core site in East Antarctica: implications for the interpretation of a water isotope record. Climate of the Past, 19, 1653–1675. https://doi.org/10.5194/cp-19-1653-2023, 2023.

Jouzel, J., Merlivat, L., and Lorius, C.: Deuterium excess in an East Antarctic ice core suggests higher relative humidity at the oceanic surface during the last glacial maximum. Nature, 299, 688–691. https://doi.org/10.1038/299688a0S, 1982.

Jouzel, J., Alley, R. B., Cuffey, K. M., Dansgaard, W., Grootes, P., Hoffmann, G., Johnsen, S.J., Koster, R.D., Peel, D., Shuman, C.A., Stievenard, M., Stuiver, M., and White, J.: Validity of the temperature reconstruction from water isotopes in ice cores. Journal of Geophysical Research Oceans, 102, 26471–26487, https://doi.org/10.1029/97JC01283, 1997.

Khan. I. (2019). Climate-related variability of isotopic records in a coastal Antarctic ice (Master's thesis). Retrieved from [http://hdl.handle.net/10579/15637]. Venice, Italy: Università Ca' Foscari Venezia.

Kim, BH., Seo, KW., Eom, J., Chen, J., and Wilson., C.: Antarctic ice mass variations from 1979 to 2017 driven by anomalous precipitation accumulation. Scientific Reports, 10, 20366. https://doi.org/10.1038/s41598-020-77403-5, 2020.

Kino, K., Okazaki, A., Cauquoin, A., and Yoshimura, K.: Contribution of the Southern Annular Mode to variations in water isotopes of daily precipitation at Dome Fuji, East Antarctica. Journal of Geophysical Research: Atmospheres, 126, e2021JD035397. https://doi. org/10.1029/2021JD035397, 2021.

Klein, F., Abram, N. J., Curran, M. A. J., Goosse, H., Goursaud, S., Masson-Delmotte, V., Moy, A., Neukom, R., Orsi, A., Sjolte, J., Steiger, N., Stenni, B., and Werner, M.: Assessing the robustness of Antarctic temperature reconstructions over the past 2 millennia using pseudoproxy and data assimilation experiments, Climate of Past, 15, 661–684. https://doi.org/10.5194/cp-15-661-2019, 2019.

Lee, H-J., and Jin, E.M.: The dominant influence of indian ocean dipole-like ocean warming on decreased precipitation over eastern East Antarctica. Front. Earth Sci. 12:1387809. doi: 10.3389/feart.2024.1387809, 2024.

Leroy-Dos Santos, C., Fourré, E., Agosta, C., Casado, M., Cauquoin, A., Werner, M., Minster, B., Prié, F., Jossoud, O., Petit, L., and Landais, A.: From atmospheric water isotopes measurement to firn core interpretation in Adélie Land: a case study for isotope-enabled atmospheric models in Antarctica. The Cryosphere, 17, 5241–5254. https://doi.org/10.5194/tc-17-5241-2023, 2023.

Lewis, S.C., LeGrande, A.N., Kelley, M., and Schmidt, G.A.: Modeling insights into deuterium excess as an indicator of water vapor source conditions. J. Geophys. Res. Atmos., 118, no. 2, 243-262, doi:10.1029/2012JD017804, 2013.

Magand, O., Frezzotti, M., Pourchet, M., Stenni,B., Genoni, L., and Fily, M.: Climate variability along latitudinal and longitudinal transects in east Antarctica. Annals of Glaciology, 39, 351–358. doi:10.3189/172756404781813961, 2004.

Markle, B. R., and Steig, E. J.: Improving temperature reconstructions from ice-core water-isotope records. Climate of the Past, 18, 1321–1368. https://doi.org/10.5194/cp-18-1321-2022, 2022.

https://doi.org/10.5194/egusphere-2025-2408
Preprint. Discussion started: 17 July 2025


Masson-Delmotte, V., Delmotte, M., Morgan, V., Etheridge, D., van Ommen, T., Tartarin, S., and Hoffmann, G.: Recent southern Indian Ocean climate variability inferred from a Law Dome ice core: new insights for the interpretation of coastal Antarctic isotopic records. Climate Dynamics 21, 153–166. https://doi.org/10.1007/s00382-003-0321-9, 2003.

Masson-Delmotte, V. S., Hou, S., Ekaykin, A., Jouzel, J., Aristarain, A., Bernardo, R.T., Bromwich, D., Cattani, O., Delmotte, M., Falourd, S., Frezzotti, M., Gallée, H., Genoni, L., Isaksson, E., Landais, A., Helsen, M.M., Hoffmann, G., Lopez, J., Morgan, V., Motoyama, H., Noone, D., Oerter, H., Petit, J.R., Royer, A., Uemura, R., Schmidt, G.A., Schlosser, E., Simões, J.C., Steig, E.J., Stenni, B., Stievenard, M., van den Broeke, M.R., van de Wal, R.S.W., van de Berg, W.J., Vimeux, F., and White, J.W.C.: A review of Antarctic surface snow isotopic composition: Observations, atmospheric circulation, and isotopic modeling. Journal of Climate, 21, 3359-3387. doi:10.1175/2007JCLI2139.1, 2008.

Matsuoka, K., Skoglund, A., Roth, G., de Pomereu, J., Griffiths, H., and Headland, R.: Quantarctica, an integrated mapping environment for Antarctica, the Southern Ocean, and sub-Antarctic islands. Environmental Modelling & Software 140, 105015. doi:10.1016/j.envsoft.2021.105015, 2021.

Mayewski, P. A., Meredith, M.P., Summerhayes, C.P., Turner, J., Worby, A., Barrett, J., Casassa, G., Bertler, N.A.N., Bracegirdle, A.C., Garabato, N., Bromwich, D., Campbell, H., Hamilton, G.S., Lyons, W.B., Maasch, K.A., Aoki, S., Xiao, C., and Tas van Ommen.: State of the Antarctic and Southern Ocean climate system, Rev. Geophys., 47, RG1003, doi:10.1029/2007RG000231, 2009.

Medley, B., McConnell, J. R., Neumann, T. A., Reijmer, C. H., Chellman, N., Sigl, M., and Kipfstuhl, S.: Temperature and Snowfall in Western Queen Maud Land Increasing Faster Than Climate Model Projections. Geophysical Research Letter, 45, 1472–1480. https://doi.org/10.1002/2017GL075992, 2018.

Medley, B., and Thomas, E.R.: Increased snowfall over the Antarctic Ice Sheet mitigated twentieth-century sea-level rise. Nature Climate Change, 9, 34–39. https://doi.org/10.1038/s41558-018-0356-x, 2019.

Meyerson, E.A., Mayewski, P.A., Kreutz, K.J., David Meeker, L., Whitlow, S.I, and Twickler, M.S.: The polar expression of ENSO and sea-ice variability as recorded in a South Pole ice core. Annals of Glaciology, 2002;35:430-436. doi:10.3189/172756402781817149, 2002.

Nardin, R., Severi, M., Amore, A., Becagli, S., Burgay, F., Caiazzo, L., Ciardini, V., Dreossi, G., Frezzotti, M., Hong, S.-B., Khan, I., Narcisi, B. M., Proposito, M., Scarchilli, C., Selmo, E., Spolaor, A., Stenni, B., and Traversi, R.: Dating of the GV7 East Antarctic ice core by high-resolution chemical records and focus on the accumulation rate variability in the last millennium. Climate of the Past, 17, 2073–2089, https://doi.org/10.5194/cp-17-2073-2021, 2021.

Nicolas, J. P., and Bromwich, D. H.: New Reconstruction of Antarctic Near-Surface Temperatures: Multidecadal Trends and Reliability of Global Reanalyses, Journal of Climate, 27(21), 8070-8093. https://doi.org/10.1175/JCLI-D-13-00733.1, 2014.

https://doi.org/10.5194/egusphere-2025-2408
Preprint. Discussion started: 17 July 2025


Nyamgerel, Y., Han, Y., Kim, S., Hong, S., Lee, J., and Hur, S. Chronological characteristics for snow accumulation on Styx Glacier in northern Victoria Land, Antarctica. Journal of Glaciology, 66(260), 916-926. doi:10.1017/jog.2020.53, 2020.

Nyamgerel, Y., Han, Y., Hwang, H., Han, C., Hong, S., Hur, S., and Lee, J.: Climate-related variabilities in the Styx-M ice core record from northern Victoria Land, East Antarctica, during 1979–2014, Science of The Total Environment, 935, 173319, doi.org/10.1016/j.scitotenv.2024.173319, 2024.

Oerter, H., Wilhelms, F., Jung-Rothenhausler, F., Goktas, F., Miller, H., Graf, W., and Sommer, S.: Accumulation rates in Dronning Maud Land, Antarctica, as revealed by dielectric-profiling measurements of shallow firn cores. Annals of Glaciology, 30, 27–34, https://doi.org/10.3189/172756400781820705, 2000.

Palerme, C., Genthon, C., Claud, C., Kay, J.E., Wood, N.B., and L'Ecuyer, T.: Evaluation of current and projected Antarctic precipitation in CMIP5 models. Climate Dynamics, 48, 225–239. https://doi.org/10.1007/s00382-016-3071-1, 2017.

Purich, A., England, M. H., Cai, W., Chikamoto, Y., Timmermann, A., Fyfe, J. C., Frankcombe, L., Meehl, G.A., and Arblaster, J.M.: Tropical Pacific SST Drivers of Recent Antarctic Sea Ice Trends. Journal of Climate, 29(24), 8931-8948, https://doi.org/10.1175/JCLI-D-16-0440.1, 2016.

Rignot, E., Mouginot, J., Scheuchl, B., van den Broeke, M., van Wessem, M. J., and Morlighem, M.: Four decades of Antarctic Ice Sheet mass balance from 1979-2017. Proceedings of the National Academy of Sciences of the United States of America, 116(4), 1095–1103. https://doi.org/10.1073/pnas.1812883116, 2019.

Rintoul, S.R., Chown, S.L., DeConto, R.M., England, M.H., Fricker, H.A., Masson-Delmotte, V., Naish, T.R., Sieger, M.J., and Xavier, J.C.: Choosing the future of Antarctica. Nature 558, 233–241 (2018). https://doi.org/10.1038/s41586-018-0173-4, 2018.

Roberts, J., Plummer, C., Vance, T., van Ommen, T., Moy, A., and Poynter, S.: A 2000 year annual record of snow accumulation rates for Law Dome, East Antarctica. Climate of the Past, 11 (5). pp. 69770. https://doi.org/10.5194/cp116972015, 2015.

Russell, A., and McGregor, G.R.: Southern hemisphere atmospheric circulation: impacts on Antarctic climate and reconstructions from Antarctic ice core data. Climatic Change, 99, 155–192. https://doi.org/10.1007/s10584-009-9673-4, 2010, 2010.

Schneider, D. P., and Steig, E. J.: Ice cores record significant 1940s Antarctic warmth related to tropical climate variability. Proc. Natl. Acad. Sci. U.S.A. 105, 12154–12158, 2008.

Schlosser, E., H. Anschütz, D. Divine, T. Martma, A. Sinisalo, S. Altnau, and E. Isaksson.: Recent climate tendencies on an East Antarctic ice shelf inferred from a shallow firn core network, J. Geophys. Res. Atmos., 119, 6549–6562, doi:10.1002/2013JD020818, 2014.

Sodemann, H., and Stohl, A.: Asymmetries in the moisture origin of Antarctic precipitation. Geophysical Research Letters, 36, L22803, doi:10.1029/2009GL040242, 2009.

https://doi.org/10.5194/egusphere-2025-2408
Preprint. Discussion started: 17 July 2025


Servettaz, A. P. M., Orsi, A. J., Curran, M. A. J., Moy, A. D., Landais, A., Agosta, C., Holly, V., Winton, L., Touzeau, A., McConnell, J.R., Werner, M., and Baroni, M.: Snowfall and water stable isotope variability in East Antarctica controlled by warm synoptic events. Journal of Geophysical Research Atmospheres, 125, e2020JD032863. https://doi.org/10.1029/2020JD032863, 2020.

Sharma, S., Ha, KJ., Yamaguchi, R., Rodgers, K.B., Timmermann, A., and Chung, E-S.: Future Indian Ocean warming patterns. Nat Commun 14, 1789 (2023). https://doi.org/10.1038/s41467-023-37435-7, 2023.

Stenni, B., Caprioli, R., Cimino, L., Cremisini, C., Flora, O., Gragnani, R., Longinelli, A., Maggi, V., and Torcini, S.: Years of isotope and chemical records in a firn core from Hercules Névé, Northern Victoria Land, Antarctica. Annals of Glaciology, 29, 106–112. doi: 10.3189/172756499781821175, 1999.

Stenni, B., Masson-Delmotte, V., Johnsen, S., Jouzel, J., Longinelli, A., Monnin, E., Rothlisberger, R., and Selmo, E.: An oceanic cold reversal during the last deglaciation. Science. 2001 Sep 14;293(5537):2074-7. doi: 10.1126/science.1059702. PMID: 11557889, 2001.

Stenni, B., Proposito, M., Gragnani., R., Flora, O., Jouzel, J., Falourd, S., and Frezzotti, M.: Eight centuries of volcanic signal and climate change at Talos Dome (East Antarctica). Journal of Geophysical Research, 107(D9), 1–14. doi:10.1029/2000JD000317, 2002.

Stenni, B., Curran, M. A. J., Abram, N. J., Orsi, A., Goursaud, S., Masson-Delmotte, V., Neukom, R., Goosse, H., Divine, D., van Ommen, T., Steig, E. J., Dixon, D. A., Thomas, E. R., Bertler, N. A. N., Isaksson, E., Ekaykin, A., Werner, M., and Frezzotti, M.: Antarctic climate variability on regional and continental scales over the last 2000 years. Climate of the Past, 13, 1609–1634, https://doi.org/10.5194/cp-13-1609-2017, 2017.

Thomas, E. R., Marshall, G. J., and McConnell, J. R.: A doubling in snow accumulation in the western Antarctic Peninsula since 1850. Geophysical Research Letters, 35, L01706, doi:10.1029/2007GL032529, 2008.

Thomas, E. R., and Abram, N. J.: Ice core reconstruction of sea ice change in the Amundsen-Ross Seas since 1702 A.D. Geophysical Research Letters, 43, 5309–5317, doi:10.1002/2016GL068130, 2016.

Thompson, D. and Solomon, S.: Interpretation of recent southern hemisphere climate change, Science, 296(5569), 895-899, 2002.

Timmermann, R., and Hellmer, H. H.: Southern Ocean warming and increased ice shelf basal melting in the twenty-first and twenty-second centuries based on coupled ice-ocean finite-element modelling. Ocean Dynamics, 63(9–10), 1011–1026. https://doi.org/10.1007/s10236-013-0642-0, 2013.

Tuohy, A., Bertler, N., Neff, P., Edwards, R., Emanuelsson, D., Beers, T., and Mayewski, P.: Transport and deposition of heavy metals in the Ross Sea Region, Antarctica, Journal of Geophysical. Research. Atmospheres, 120, 10,996– 11,011. doi:10.1002/2015JD023293, 2015.

Turner, J., R.A., Bindschadler, P., Convey, G., di Prisco, E., Fahrbach, J., Gutt, D.A., and Hodgson, P.A.: Mayewski and C.P. Summerhayes (editors). (2009). Antarctic climate change and the environment. Cambridge: Scientific Committee on Antarctic Research.

https://doi.org/10.5194/egusphere-2025-2408
Preprint. Discussion started: 17 July 2025


Turner, J., Phillips, T., Thamban, M., Rahaman, W., Marshall, G. J., Wille, J. D., Favier, V., Winton, V.H.L., Thomas, E., Wang, Z., van den Broeke, M., Hosking, J.S., and Lachlan-Cope, T.: The dominant role of extreme precipitation events in Antarctic snowfall variability. Geophysical Research Letters, 46, 3502–3511. https://doi.org/10.1029/2018GL081517, 2019.

Uemura, R., Matsui, Y., Yoshimura, K., Motoyama, H., and Yoshida., N.: Evidence of deuterium excess in water vapor as an indicator of ocean surface conditions, J. Geophys. Res., 113, D19114, doi:10.1029/2008JD010209, 2008.

Vance, T. R., Roberts, J. L., Moy, A. D., Curran, M. A. J., Tozer, C. R., Gallant, A. J. E., Abram, N. J., van Ommen, T. D., Young, D. A., Grima, C., Blankenship, D. D., and Siegert, M. J.: Optimal site selection for a high-resolution ice core record in East Antarctica, Climate of the Past, 12(3): 595-610, 2016.

Yuan, X.: ENSO-related impacts on Antarctic sea ice: a synthesis of phenomenon and mechanisms. Antarctic Science. 2004;16(4):415-425. doi:10.1017/S0954102004002238, 2004.

Zhang, P. and Duan, A.: Connection between the Tropical Pacific and Indian Ocean and Temperature Anomaly across West Antarctic. npj Clim Atmos Sci 6, 49. https://doi.org/10.1038/s41612-023-00381-8, 2023.

Zhang, L., Ren, X., Cai, W., Li, X., and Wu, L.: Weakened western Indian Ocean dominance on Antarctic sea ice variability in a changing climate. Nat Commun 15, 3261 (2024). https://doi.org/10.1038/s41467-024-47655-0, 2024.

https://doi.org/10.5194/egusphere-2025-2408
Preprint. Discussion started: 17 July 2025


**Table captions**

**Table 1.** Descriptive statistics for the annual means of the GV7-C ice core data.

**Table 2.** Linear regression analysis for $\delta^{18}O$ and $\delta D$ from the GV7-C ice core.

**Table 3.** Linear regression analysis for $\delta^{18}O$ and *d*-excess from the GV7-C ice core.

**Table 4.** Comparison of the mean snow accumulation rate from the GV7-C ice core with previous records in this location.

**Table 5.** Summary of observed correlations between the GV7-C ice core and the climate variables from the ERA5 reanalysis data by period (annual [ANN] and the DJF, MAM, JJA, and SON seasons) for the period 1957–2013 CE.

**Table 6.** Loadings of the variables for the first four principal components (PCs) of the PCA analysis conducted with the data for 1957–2013. Larger values ($r > 0.3$) are marked in bold.

**Table 7.** Pearson's correlation coefficients (r) between the three- and five-year average (in parentheses) and running averaged time series of the GV7-C ice core records and the climate variables for the period 1957–2013. Larger values ($r > 0.3$ at $p < 0.05$) are marked in bold. SIE (EA) and SIE (RA) denotes sea ice extent over East Antarctica and the Ross-Amundsen Sea sector.

**Table 8.** Pearson's correlation coefficients between the three- and five-year average (in parentheses) and running averaged time series of the GV7-C ice core records and the climate variables for the period 1872–2013 CE. Larger values ($r > 0.3$ at $p < 0.05$) are marked in bold.

https://doi.org/10.5194/egusphere-2025-2408
Preprint. Discussion started: 17 July 2025


**Figure captions**

**Figure 1.** Location of the GV7-C ice core and other ice core sites in East Antarctica. The red lines indicate the median sea ice concentration in February and the purple line represents the same for September based on data from 1981–2010 CE (Fetterer et al., 2016). The map was generated using QGIS software with Quantarctica3 project data (Matsuoka et al., 2021).

**Figure 2.** Temporal variation in the SA (bottom panel), $\delta^{18}O$ (middle panel), and *d*-excess (top panel), with the horizontal black line indicating the overall mean. The thick black lines represent the 5-year running average. The blue and red lines (arrows) indicate the periods that are higher or lower than average for at least four continuous years.

**Figure 3.** Comparison of the standardized profiles (grey lines) for SA, $\delta^{18}O$, and *d*-excess with the climate variables for 1957–2013. The red and blue lines indicate the 3- and 5-year running average. The vertical red shading indicates periods with large $\delta^{18}O$ values.

**Figure 4.** Comparison of the 5-year running average for SA, $\delta^{18}O$, and *d*-excess with the IOD, SST anomaly of the southeastern Indian Ocean (SST-SEIO), SST anomalies over the Southern Hemisphere, the SAM, and Nino3.4 for 1872–2013 CE. The SAM index is presented with the annual mean (thin blue line) and the neutral (at zero) horizontal line. The thin purple line indicates the annual mean of Nino3.4. The thin grey line represents the annual mean of the SA, $\delta^{18}O$, and *d*-excess. The blue and red lines (or arrows) indicate the periods with a higher or lower than average SA, $\delta^{18}O$, and *d*-excess over at least four consecutive years. The gray shading corresponds to the period after 1957. The linear trend in $\delta^{18}O$ during the 1782–1845 CE period is represented by the black line.

**Figure 5.** Spatial correlation of *d*-excess with annual SST variability for (a) 1979–2013 CE, (b) 1957–2013 CE, and (c) 1854–2013 CE. The scale bars indicate Pearson's correlation coefficient (r) at $p < 0.05$. This figure was generated using Climate Reanalyzer (https://climatereanalyzer.org/) from the Climate Change Institute, University of Maine, USA.